Response to Reviewers' comments on the manuscript:

Simulating the Variations of Carbon Dioxide in the Global Atmosphere on the Hexagonal Grid of DYNAMICO Coupled with the LMDZ6 Model

Z. Lloret, F. Chevallier, A. Cozic, M. Remaud, Y. Meurdesoif

We would like to thank the reviewers for their thorough reading of our manuscript and their constructive feedback. The present document contains the replies to the general and specific comments. Replies to Reviewer 2 start on page 8. The original text from the manuscript is quoted in blue, and the amended version when present is in red. The new version of the manuscript with track changes is attached at the end of this document.

Replies to comments by Reviewer 1

General comments by Reviewer 1 (GC1)

GC1.1 *This paper presents a comparison of global CO2 atmospheric transport using two different configurations of the LMDZ general circulation model. The difference between the two configurations is that one uses the hexagonal grid of the DYNAMICO core (ICO) and another uses the longitude-latitude grid (REG). The main conclusion of the paper is that the ICO configuration achieves a similar accuracy as REG while reducing the computation cost by about 20%.*

My main concerns of this paper are:
• Submitted as "Development and technical paper", this paper does not contain model development nor any substantial description of the model used in the comparison except for the references provided. In general, the model description in this paper lacks the necessary details.

Authors:

We modified Section 2.1 to make it clear what is new in this paper and the development we did. We divided the section in two subsections and an overhead. The overhead briefly presents the two configurations, and which models they each use. The first subsection 2.1.1 presents the details of the individual models used in our coupled configurations, based on our references. The second subsection 2.1.2 presents the new configuration in more detail.

We also added information in the introduction to better frame the context of this paper.

GC1.2 *Comparisons of the two model configurations (REG and ICO) are needed to make this paper valid. At the coarse resolution of 2.5◦ × 1.25◦, there is no clear advantage of using ICO over REG. Similar*

global CO2 atmospheric transport model simulation at higher horizontal resolution can be found at [1, 2, 3].

Authors:

Comparison with our reference configuration, which used the 2.5° × 1.25° resolution on a regular latitude-longitude grid was a necessary first step in evaluating the performance and quality of the new ICO configuration. Since this study was exploratory in nature and is the first use of DYNAMICO in a coupled GCM, doing this comparison at a higher, an unexplored resolution would have necessitated preliminary studies to increase the resolution of the reference configuration. The choice was made to work first on integrating the new DYNAMICO dynamical core before any future work on resolution increase. This choice was motivated in large part by the context of the upcoming Coupled Model Intercomparison Project Phase 7 (CMIP 7), for which the choice was made for models using the LMDZ GCM to switch to DYNAMICO.

Nonetheless, we agree that at least a proof of concept at higher resolution is needed to support the validity of our choice and to drive the point of our study that new innovative grids provide advantages compared to regular latitude-longitude grids. To that point, we conducted computing performance tests comparing the two configurations at a higher resolution, corresponding to 1.4° × 0.7° for the regular configuration, and a resolution for ICO that doubled, corresponding to around 1.25° × 0.625° at the equator.

This comparison was added to Section 3.2.1, and results were discussed in the new Section 3.2.2. Results show that while at the lower resolution computing speed increase was only on the order of the savings in grid size. At this higher resolution, where both configurations have the same number of grid cells, ICO is much faster than the regular configuration, exhibiting much better scaling across resolutions.

GC1.3 *I could not figure out whether the integration of the Dynamico core to LMDZ for tracer transport is implemented in this paper or in the previous study by [4]? In Line 47, it states that "We build on the dynamical core Dynamico (Dubos et al., 2015), which has recently been integrated into LMDZ", yet between Sections 2.1.1 and 2.1.2, it appears that the REG has the older dynamical core. If the implementation of Dynamico core to LMDZ for CO2 transport is done in this paper, a detailed description is needed. If it is done in [4], what is the scientific contribution of this paper in terms of model development?*

Given the above concerns, I think this paper needs substantial revision before it can be considered for publication at GMD.

Authors:

The paper [4] (Hourdin et al., 2020) presented LMDZ6A, the GCM we use as a reference in our study. For the reference configuration REG, the dynamics and physics of LMDZ6A are used and coupled with a chemistry and land model. Our new configuration ICO replaces the dynamics of LMDZ6A with the dynamical core DYNAMICO and couples it to the already existing physics of LMDZ6A. The study [4] does not use DYNAMICO in any way.
The sentence *"which has recently been integrated into LMDZ"* was confusing and has been removed. Furthermore to better explain the developments done to implement DYNAMICO into the LMDZ GCM, we modified Section 2.1 extensively and also added information in the introduction to better frame the context of our developments.

Specific comments by Reviewer 1 (SC1)

Reviewer's comments	Replies from Authors	Modified text
SC.1.1 -Line 22-23. Given the fact that both the ICO and REG simulations used in this study have a horizontal resolution of about 2.5◦ × 1.25◦, I do not see how the study "emphasize the importance of .... high-resolution innovative grids...".	We removed the words high-resolution from the sentence since our study does not look at the effect of higher resolution on our understanding of the global carbon budget.	This study emphasizes the importance of advanced modeling approaches and ~~high-resolution~~ innovative grids in enhancing our understanding of the global carbon cycle and refining climate models.
SC.1.2 -Lines 43-45. The authors state that model simulations using regular longitude-latitude grids have resolution clustering problems which leads to computing bottlenecks caused by significant data communication. "In this paper, we are addressing this specific issue...", however in Lines 249-250, "This speedup is comparable to the reduced number of cells in ICO. For our spatial resolution, it seems that other differences such as the absence of a polar filter for ICO did not significantly improve the computational speed." My understanding is that the current simulation comparison at the coarse resolution of 2.5◦ × 1.25◦ does not prove the ICO configuration has a substantial advantage over the REG except for the reduced number of cells	We refer to our answer to **GC1.2**, we agree that comparison at a higher resolution was necessary. We did so and reported the results in Section 3.2.1, and discussed the results in Section 3.2.2.	

(about 20%). A comparison at higher horizontal resolutions is needed to support the main points of this paper.		
SC.1.3 -Line 46: “Such a solution has been explored by few models so far,...” This statement is not up-to-date: Unstructured grids have been used for simulating global atmospheric CO2 transport in several studies, such as [2, 3]	The sentence has been reworded, and studies using such models for atmospheric CO_2 transport have now been cited.	Such a solution is gaining popularity in recent years ~~has been explored by few models so far~~, either for use in Earth system models, transporting tracers or directly for atmospheric inversion (Niwa et al., 2017; Giorgetta et al., 2018; Sakaguchi et al., 2020; Zheng et al., 2021).
SC.1.4 -Line 55: “Coupling it to the LMDZ GCM also represents the first step towards the use of Dynamico for inverse modeling”. I guess you meant inverse modeling of CO2. Please specify.	Indeed, this is now specified.	Coupling DYNAMICO ~~it~~ to the LMDZ GCM also represents the first step towards the use of DYNAMICO for inverse modeling of CO_2.
SC.1.5 -Lines 68-72. As CO2 is modeled as a tracer, the chemical processes in INCA are not applied. Please state this explicitly.	This is now explicitly stated.	In our study, these chemical processes are not applied to the CO_2 tracer.
SC.1.6 -Line 90. Please specify “our resolution”	The sentence was removed (see review 2).	
SC.1.7	This was forgotten across revisions during the editing process, this has been replaced with simply ICO.	

-Line 94. “ICOLMDZORINCA”. The acronym is used here without being previously defined.		
SC.1.8 -Line 99. Please clarify whether the atmospheric dynamics used for CO2 transport described in this study is hydrostatic or non-hydrostatic. It is not clear the way it is presented here.	In this study, the atmospheric dynamics are hydrostatic, a sentence has been added here to make it explicit.	In this study, the hydrostatic mode was used.
SC.1.9 -Lines 105-107. The two sentences appear to be contradictory: the first states that the transport equations do not use any information from the momentum equations, while the second states that the kinematics handle the transport of mass, potential temperatures, and tracers using the mass fluxes computed by the dynamics.	We removed the first sentence.	~~Kinematics and dynamics were separated as much as possible so that transport equations do not use any information from the momentum equations.~~
SC.1.10 -Line 107. Since both the REG and ICO use the same atmospheric model LMDZ (with different dynamical cores), this sentence is a bit confusing. Do you mean “does not differ from vertical transport from the REG configuration”? See line 113.	This is indeed what was meant, and the sentence has been corrected to reflect it.	The vertical transport uses a slope-limited Van Leer's scheme (Van Leer, 1977) and does not differ from the REG configuration ~~vertical transport of LMDZ.~~
SC.1.11	The surface emissions of CO_2 are indeed prescribed, and read by INCA, modifying the	In our configurations, tracers, such as CO_2, are outputted ~~modeled~~ by INCA

-Line 124-125. Judging from this sentence, it appears that CO2 fluxes are prescribed (using CAMS). However, in line 68, it states that “tracers, such as CO2, are modeled by INCA”. Please clarify the seemingly contradictory statements.	concentration of this tracer in the INCA model. We replaced the word “modeled” in this sentence by “outputted”, which is more accurately the message meant to be carried by this sentence.	
SC.1.12 -Line 126-127. Remaud (2018) tested the impacts of two different versions of LMDZ physics on CO2 atmospheric transports and these tests all used the latitude-longitude grid. I do not understand how the authors reached the conclusion of “we consider that this imprint hardly affects our conclusions” as the ICO simulation used a hexagonal grid.	The prescribed fluxes are interpolated on the new grid, erasing that imprint at low scale while conserving the mass locally.	
SC.1.13 -Line 128. What are the “boundary files”? Please explain.	The types of files used have now been specified (aerosol, oxydants and ozone concentration, solar forcing, land use maps).	The boundary files used for the two simulations were identical (aerosol, oxydants and ozone mole fraction, solar forcing, land use maps).
SC.1.14 -Lines 149-151. It is not clear to me how “This selection accounts for the usual failure of ..”.	By selecting data differently between high-altitude and low-altitude surface stations, we ensure that the cases described here are avoided. To avoid confusion with flask and airborne data, the sentence about them has been moved after this one.	
SC.1.15 -Line 382. The causes that both ICO and REG configurations provide inadequate modeling of	This is true, and we added this information to the sentence to clarify it.	Nevertheless, both configurations provide an inadequate modeling of synoptic variability, as the local high-frequency emissions are poorly

synoptic variability most likely also include the horizontal resolution used in the simulations.		constrained and the horizontal resolution is still too coarse.
SC.1.16 -Lines 392-393. This sentence is quite confusing. Probably it can be better phrased.	The sentence has been reworded.	ICO provides a more homogeneous grid compared to the grid clustering at the poles of a regular latitude-longitude grid.
SC.1.17 -Line 398-399. It is not clear to me what you meant by the “damping the induced increase of the code time-to-solution”. Please clarify.	The choice of words might have been poor. The sentence has been replaced.	[...] while limiting the induced increase in computational cost ~~of the code time-to-solution~~.
SC.1.18 -Line 40: “e.g., the kilometric resolution of the current space-born...”. Do you mean the computational cost of model simulation at kilometer resolution?	Yes, the resolution of spaceborne observations in this case was to be used as a reference exemple. The sentence has been reworded to avoid confusion.	[...] not enough to close the gap between model resolution ~~with~~ and, e.g., the kilometric resolution of the current space-borne observations.
SC.1.19 -Line 113: Is this one-sentence paragraph intentional?	This indentation error has been corrected.	

Replies to comments by Reviewer 2

General comments by Reviewer 2 (GC2)

GC2.1 *This paper presents a comparison of two general GCMs, LMDZORINCA (REG), which is an established setup, and ICO, which is the novel version presented in this manuscript. The authors test the effects on simulated CO2. Their main conclusion is that a similar performance is found between the two setups, but that ICO has a 20 percent less CPU cost by utilizing a smaller/reduced grid.*

Although this comparison in itself can be an interesting step in improving the transport model performance, the current manuscript is not convincing in showing that this development is, in fact, an improvement of the REG setup, and it would require substantial revision before it could be considered for publication. Below are several general and specific comments that could help to improve the manuscript.

The manuscript seems to contain relatively little innovation. The abstract suggests that ICO is the innovation that is being presented. Section 2.1.2 seems to introduce the ICO concept for the first time, but no explanation is given on how this coupler works. For example, what time stepping is used, and why. How are these different in REG? Currently, it is not clear which innovation is exactly documented by this manuscript. Either the innovation was already described in previous studies (shown by several references to previous work, e.g., on line 82), or if this is the first manuscript presenting, the description would need to be more elaborate. The methodology section would need to be rewritten so that it is clear which information is new, and only include information from previous work if it is necessary to understand this manuscript.

Authors:

This paper's goal is to present the ICO configuration of LMDZ and to make it public. This is indeed the first time that DYNAMICO has been successfully used in an Atmospheric GCM, and therefore its first use for the simulation of a real tracer in the global atmosphere.

We added explanations on how the coupler between DYNAMICO and LMDZ works to section 2.1.2, the choice of the time step was identical to the one of the REG configuration, with the time step of the dynamics being smaller than that of the physics. Half of the 15 minutes of the physics for our resolution.

The studies such as the one referenced on line 82 (Remaud et al., 2018) relate to the development and evaluation of the LMDZ GCM with its regular grid. They serve to establish the basis of our reference REG configuration. None of them include DYNAMICO in any way, see Table GC1.1.

Section 2.1 has been rewritten and divided into subsections to clarify the parts of our study that are new and those that simply describe the already developed models that we use. We also modified the introduction to better frame the context of our study.

Reference	Development
Hourdin et al., 2020 Remaud et al., 2018	Presentation of the LMDZ6A GCM, used in the REG configuration. Evaluation of the tracers with LMDZ6A
Dubos et al., 2015 Our study	Creation of DYNAMICO, stand-alone dynamical core Implementation of DYNAMICO with the LMDZ GCM (new ICO configuration) Evaluation of CO_2 tracer transport

Table GC1.1 History of the developments of the LMDZ GCM.

GC2.2 *In the manuscript, several problems are identified which may explain the cases where ICO performs worse than REG in terms of simulating CO2. However, these are either not solved (mass conservation in Section 3.1, see also major concerns below), or indicated to be beyond the scope of this study (Section 3.3 temperature profiles, and their potential impact on the results presented in Section 3.5). It is therefore not clear if and why the authors would recommend using ICO instead of REG. Reading the manuscript as is, it seems that REG shows better performance, and yet the authors suggest continuing the development of ICO, and seem to indicate that ICO is, in fact, showing equal performance compared to REG. How are future developments going to impact the results? If there are major updates in the pipeline, would it not be better to merge those with the current manuscript so that it does not lose its relevance after those updates?*

Authors:

The issue of mass conservation is explained in detail in the answer to **GC2.4**.

As also discussed in the answer to the next general comment **GC2.3**, DYNAMICO represents the cornerstone of future development of the atmospheric models from Institut Pierre-Simon Laplace (including its Earth-system model), in the context of the overarching long-term strategy to adapt models to new supercomputers and to pave the way for future increases in resolution.

Our study is the first implementation and evaluation of a coupled configuration using DYNAMICO, it represents an important and necessary step for future use of this configuration and similar ones that will also use DYNAMICO. Further tuning and an eventual increase in this configuration's resolution will occur. DYNAMICO is expected to slowly become the go-to dynamical core for the LMDZ GCM thanks to its much better scaling at high resolution and will be improved by many different people (in particular for future use as part of CMIP7) for an expected long period of time.

However, since no exact time frame for these upcoming changes can be produced, and the authors of this study will not be responsible for all of these developments, we had to set limits and present the results as they stand at this time, for a configuration that is operational.

We added a paragraph in the introduction and modified several sentences to better explain how our study fits into this overall development.

The only major difference between the ICO and REG simulations of CO_2 shown in the previous version of the manuscript was in the comparison to AirCore measurements, showing the ICO configuration performing worse than the REG configuration. However, following a discussion with Bianca Baier from NOAA in the meantime, we found that the initial AirCore dataset we used contained altitude determination errors (see the answer to **SC.2.31** for details). We replaced it with a newer version of the dataset exempt from these errors. This changed the results of the comparison between our two configurations and the measurements. With this updated dataset, the ICO configuration has very similar results to the REG configuration (see amended Section 3.5.2).

Therefore, for CO_2 tracer transport, the ICO configuration performs generally as well as the REG configuration. Furthermore, as we explain in our answer to the next general comment **GC2.3** as well as in our answer to **GC.1.2**, improvements in performance, from a reduced grid size at our reference resolution and from improved scaling at higher resolution provide a strong incentive to use DYNAMICO and to continue its future development.

GC2.3 *Also, a discussion of the performance is missing, and the manuscript would benefit from having a discussion section included. In such a section, the authors could go more in-depth into the outcomes of the comparison and the implications. Currently, there is no comparison to the GPU version mentioned in line 40. It would be highly recommended to also include a comparison to that version, especially also in terms of computational efficiency. It is not clear where these two innovations stand with respect to each other. Also, the position compared to other models could be discussed, since the new transport scheme benefits mainly from reducing the number of computations that are required, which is comparable to reduced grids that other models use (see e.g. Petersen 1998).*

Authors:

We agree that a more in-depth discussion of the computing performance of the configurations was needed to support the main points of the study properly. We did so by adding a new Section 3.2.2, and more importantly by performing tests to compare the configurations at a higher resolution as suggested in **GC1.2**.

The GPU model described in Chevallier et al. 2023 and referenced in line 40 is an offline model running on pre-computed mass fluxes. It is not comparable to our configurations since it uses the REG configuration outputs as input, for use in inverse modeling. Since this sentence was confusing, we reworded it.

Furthermore, since the position of our configurations was not sufficiently clear, in particular the overall development strategy regarding future GPU use, resolution increase, and the role of DYNAMICO in this, we reworded parts of the introduction to better explain it.

By performing tests at a higher resolution, where both configurations have identical grid cell count and so perform the same amount of calculation, we now show that DYNAMICO enables much better scaling and performance.

GC2.4 *Currently, it is not clear what the reason is for the violation of mass conservation. I would agree that the amount of mass being lost is indeed small and not directly relevant for CO2 inversion studies. But for a technical evaluation study such as presented in this manuscript, it is vital to know the origin and whether the irrelevance can be safely extrapolated, e.g., when moving towards a higher resolution.*

Authors:

We studied the issue of mass conservation in more detail following this comment to find which of the models or couplings (see new Fig. 1) is responsible for this small defect. To that end, we verified mass conservation inside timesteps to ensure that no mass loss was incurred from routines in the dynamics (whether that is with the regular grid for LMDZ or in DYNAMICO) or when calling and interfacing with the physics. We find that these models perfectly conserve mass to machine precision, which is consistent with their expected performance when evaluated independently. The problem therefore is a discrepancy between the time-integrated values of emissions and mole fractions of our tracer coming from our couplings or parameters. But given that it was not necessary to solve for our study and was already present in the REG configuration, we did not investigate it further because of time constraints.

GC2.5 *The technique used to evaluate the seasonal cycle is not explained. The curve-finding procedure that was used is not specified (line 169). It is therefore not clear how conclusions can be drawn based on the seasonal cycle. What is the used criterion for a good fit and a bad fit? What are the residuals; do they still contain a trend or a seasonal cycle? What about the year-to-year variability? I think it would be relevant here to show the outcomes of the finding routine for both setups. Based on this, you may wish to introduce a rejection criterion for your final conclusions: if the original observed data is not fitted well enough, which I hypothesize to be the case for GIC/UTDBK and also CPT (as shown in figure 6 in the manuscript), it is not informative to see how the model performs there; it is just showing that the curve-finding routine that is applied is not sufficient to yield a good answer (in other words, for those sites, I don't think we are looking at the REG/ICO's failure to reproduce the seasonal cycle but to the capacity of the curve-finding to perform a good fit). It is also good to check whether the quality of the seasonal cycle is due to feedback within the model between meteorology and the land surface model or is it related to the transport dynamics?*

Authors:

We expanded on the description of the curve-finding procedure to clarify it. We previously did not filter stations based on the quality of the fits, this is now the case, and we only keep stations where the curve fit of the measurements has a coefficient of determination over 0.75.
With this criterion, the stations UTDBK and GIC for example were excluded, but CPT measurements had a good enough fit to be kept. This changes the overall statistics and tends to make the configurations even more similar to each other. We modified the text accordingly.
The residuals do not seem to contain a trend or seasonal cycle that we could discern, see **Fig. GC.2.5** for an example.

Since we average the seasonal cycles over the years, we do not get year-to-year variability by design, which would require a different approach.
Concerning the role of the feedback between meteorology and the land surface model vs. the transport dynamics in the quality of the seasonal cycle, the meteorology-land surface coupling has not been changed between the two model versions and therefore we do not expect this feedback to evolve.

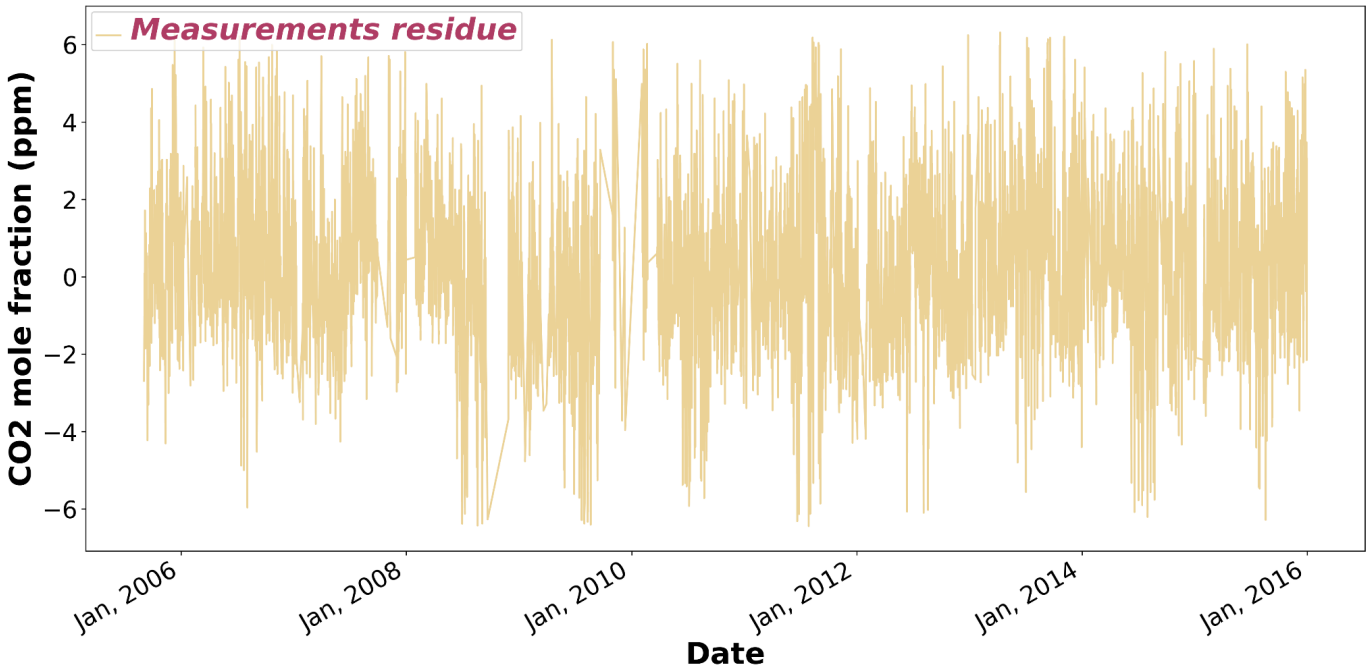

Figure GC2.5: Residual of the CO_2 mole fraction of measurements at station SPL after curve-fitting.

Specific comments by Reviewer 2 (SC2)

Reviewer's comments	Replies from Authors	Modified text
SC.2.1 It would be useful to include tables to help better understand the parallelization schemes and how they lead to a comparable setup, including which runs are performed for what results.	A table was added at the end of Section 3.2 to better explain the processing setup.	
SC.2.2 Figures 5, 7, and 8: Since the main difference between the models is the resolution towards the poles, it would be useful to see the differences by latitude. I would suggest ordering the	The figures have now been ordered by latitude on their x-axis. The statistics by latitude bands did not differ from the overall statistics. A figure of the bias of the annual gradient of	

stations by latitude. Also, aggregated statistics by latitude bands would be useful too.	aggregated per latitude band was added (Fig 8)	
SC.2.3 Line 54: What does coupled configurations mean? What is coupled to what? Maybe a block diagram of both coupled configurations could illustrate the differences between the setups?	A block diagram was added (new Fig. 1) to better explain the configurations, the role of each model, and how they interface with one another. The sentence was reworked to remove the word “coupling” since it was confusing at this place.	This paper evaluates the ability of this new configuration ~~coupling~~ of the LMDZ GCM using the DYNAMICO dynamical core to transport a long-lived tracer like CO_2.
SC.2.4 Line 61: The abbreviations are too long to be easy to read. Could you add dashes like in the full name in line 66?	The code name of the coupled model has been changed to “REG” to be consistent with the rest of the paper. The change has also been done for ICO L.94.	
SC.2.5 Lines 79-80: It is unclear how the "mix of finite difference and finite volume" affects either the primitive equations or the transport equations. Do both transport and the primitive equation use a mixed approach? Or does the primitive equation use a finite difference and the transport finite volume, and is the total model therefore considered a mix? Is this relevant e.g. in relation to mass conservation?	The sentence was reworked to simplify it since it was not relevant to the overall message.	The dynamical core of LMDZ discretizes ~~is a mix of a finite difference and finite volume discretization~~ on the sphere of the primitive equations of meteorology and of transport equations (Hourdin et al., 2006, 2013).

SC.2.6 Line 86: Is the explanation of parallelization required here?	Given that we are describing our model, it feels important to also explain in detail the parallelization scheme, however, the sentence relating to the number of processors used does seem out of place. More information on parallelization was added to Section 3.2 as discussed above with the addition of a table.	~~For LMDZ at our resolution the optimal compromise between resources and performance is achieved by using 71 MPI processes with 8 OpenMP threads running on 568 cores (Hourdin, 2020).~~
SC.2.7 Line 90: “our resolution” is unclear, but this is specified in lines 134-137, and could be moved up.	The sentence was removed (see above comment).	
SC.2.8 Line 102: What does “coarser” mean? How much?	Precision was made that we are talking about “spatial resolution”, and we added a sentence after this one to explain the process and how it relates to cell size. However, quantifying these differences would be premature in this section of the paper since it depends on resolution and latitude, while in this section we are presenting the configurations in a more generalized way.	The cells have similar areas across the globe, from the equator to the poles, unlike in the regular longitude-latitude grid where cell size gets systematically smaller when approaching the poles.
SC.2.9 Line 110: Here, further details on the parallelization scheme would be useful.	We replaced the paragraph to explain the parallelization scheme in much more detail and also added a figure for illustration.	The global mesh used in the ICO configuration is partitioned into 10 quadrilateral clusters of similar size to map the sphere. Each quadrilateral is paved with the same number of hexagonal cells, depending on the chosen resolution. It can be subdivided

		along two directions, i and j, thus generating sub-tiles in the form of parallelograms composed of $iim \times jjm$ hexagons (Fig. 3). MPI parallelism is achieved by distributing the sub-tiles thus created to each MPI process, the optimum performance being achieved for sub-tiles of identical size and with only one sub-tile per MPI process. When solving the various numerical schemes of the dynamic core, the data required at the domain boundaries is transferred by asynchronous MPI calls from one sub-tile to another. OpenMP parallelism operates through shared memory, distributing computational iterations on vertical levels over threads created within an MPI process, in a similar fashion to the REG configuration.
SC.2.10 Line 120: I would rephrase this to a simpler sentence: "In both configurations, the large-scale atmospheric circulation was nudged to the 6-hourly ERA5 reanalysis for wind."	The suggested change was done, but we kept the information about the relaxation time given its importance.	In both configurations, the large-scale atmospheric circulation was nudged to the 6-hourly horizontal winds from the ERA5 reanalysis (Hersbach et al., 2020) with a relaxation time of 3 hours.
SC.2.11 And why are the other parameters, like temperature not nudged? Could that (partially) solve the stratosphere and troposphere bias?	Nudging to horizontal winds forces the model to simulate the actual meteorology rather than a climatological one, as is done, e.g., for CMIP simulations. However, the idea is not to inhibit the online model and transform it into an offline one	

	that would simply add more variables to the ERA5 ones. Nudging to other variables would also hide model issues and biases that we actually want to reveal here. Lastly, the specific nudging to reanalysis temperature damps convection by stabilizing the temperature profiles and therefore degrades some aspects of the tracer transport realism.	
SC.2.12 Line 122: Mixing ratios is not the correct term to use; this should be replaced by mole fractions (also in other lines in the text).	This has been corrected throughout the text.	
SC.2.13 Lines 123-124: Could you specify the prior fluxes used? In line 226, it is mentioned that the prior fluxes are relevant, but they are not known to the reader. For example, the prior fluxes might partially explain the seasonalities that are presented.	The prior fluxes used by the CAMS global inversion version 20r2 are available on the Copernicus website, but we added them to the text for easier reference.	Prior fluxes used for this product were GCP-GridFED version 2021.2 for anthropogenic emissions (Jones et al., 2021), GFED 4.1 inventories for biomass burning, ocean fluxes from Chau et al. (2022) and climatological biosphere-atmosphere fluxes from an ORCHIDEE simulation, version 4.6.9.5.
SC.2.14 Line 142: Have you assessed the impact of the used sampling scheme? There can be substantial horizontal and vertical gradients in the simulated CO2 mole fractions. If you want to assess how these two simulations perform,	The vertical grid is identical between the two configurations. We also checked that horizontal sampling does not significantly affect the results for our studied metrics.	

especially at the surface, the two grids are very different, so the sampling scheme can be relevant.		
SC.2.15 Line 144: Since you are using the observations from this obspack product elaborately in the manuscript, it would be appropriate to contact the PIs of the datasets to discuss how these should be acknowledged. Currently, only Jungfraujoch and Aircore are specifically mentioned in the acknowledgments, but JFJ is not shown explicitly, while other stations are, e.g., in Figure 6.	We contacted all PIs that contributed to the Obspack dataset before submission. Since the start of the editing process a few more have answered and recommended to us better ways to properly acknowledge their work. We have followed their recommendations. This has led us to add a few citations in L.144.	We used the high-quality measurements of the CO_2 GLOBALVIEWplus v8.0_2022-08-27 ObsPack database (Schuldt et al., 2022, Miles et al., 2017, Miles et al., 2018, ICOS RI, et al., 2023, Lan et al., 2023). For AirCore, we used the dataset from NOAA Version 20230831 (Baier et al., 2021).
SC.2.16 Line 152: The explanation of the AirCore technique is not fully correct. It does not take “many successive samples of the ambient air when descending.” It rather takes a single sample while descending and utilizes the length of the tube to preserve the vertical gradients as much as possible (affected by diffusion) to obtain a vertical profile. Either rephrase or consider if the explanation is needed at all. What matters for the manuscript is that it provides a vertical profile.	The explanation might not be needed at all, the sentence has been removed.	~~AirCore (Karion et al. 2010) is an atmospheric sampling system consisting of an open-ended steel tube launched from an aerial platform and that collects many successive samples of the ambient air when descending.~~

SC.2.17 Line 171: Typo in 19080.	Amended.	
SC.2.18 Line 176: This section could benefit from describing the calculations with a couple of equations.	We added equations in Section 2.4 to better illustrate the calculations of each metric.	
SC.2.19 Line 178: It is better to consistently use mole fractions rather than concentrations (nor mixing ratios).	The change has been made throughout the paper.	
SC.2.20 Line 214: The mass conservation issue depends on the advection scheme used and the extent to which mass balancing is applied. Could you elaborate on how these two components affect either the ICO simulation or the REG simulation? This information is relevant for the discussion. It is essential to understand the process behind the acceptable loss of mass, especially when considering a higher model resolution with ICO.	No mass fixing is used in either configuration. We addressed the issue of mass conservation in more detail in the answer to **GC.2.2**.	We verified that the routines in the LMDZ physics and in the dynamical cores of both configurations perfectly conserved mass. Therefore, the small mass difference comes from discrepancies between the time-integrated values of emissions and mole fractions of our tracer, but we did not investigate it further given its negligible impact in our study.
SC.2.21	We explained the aforementioned abbreviations and standardized the notations	To do that, we calculate Δm, the observed increase in the total amount of atmospheric CO_2 over a certain period

Line 219: Several of the abbreviations in the equations are not explained in the text. What is the superscript ‘e’? What is ‘emi’? Please check these abbreviations. Also, the notations are not standardized; for example, chemical elements should not be italic. Mass is recommended to be written with a small 'm', not capital. See IUPAC Green Book.	following the recommendations of the IUPAC Green Book as suggested.	of time. In Equation (1), superscript e corresponds to the end time step of a given period studied, and i is the initial time step. We multiply the CO_2 mass fraction w with the dry air mass m_{air} in each cell and sum it over the whole grid (N cell). We then separately calculate the total emitted mass of CO_2 over a period of time, $m^{emi}_{(CO_2)}$ in Equation 4, by multiplying the surface fluxes q with the area of each cell A^n and summing it over time. The difference between these two values, m_{loss} in equation 3, is the total mass of atmospheric CO_2 lost or gained by our model over a certain period of time.
SC.2.22 Line 226: As mentioned before, these surface fluxes are not described in Section 2.2.	See answer to **SC.2.13**	
SC.2.23 Lines 247-248: I would be interested to know the comparison to the GPU version of Chevallier et al. 2023.	The model described in Chevallier et al. 2023 is an offline model running on pre-computed mass fluxes provided by the coupled model REG that is used as a reference in this study. It is essentially a stripped down version of LMDZ containing only the necessary routines for transporting CO_2 and interfacing it in an inverse system. A comparison of computational performance between these two very models	

	would therefore not be relevant for our topic here.	
SC.2.24 Line 257: This difference of 10 K that is not shown in the figure: which is better, the REG or ICO setup?	Neither of the two configurations match the ERA5 profiles, and we cannot judge which one is better strictly from this average metric.	
SC.2.25 Line 289: Considering the RMSE and looking at figure 4, I would not say the ICO has a slightly lower overall bias, since the difference in bias is probably insignificant considering the total spread of the data. They are both significantly different from the 1:1 correspondence line, but not from each other. Checking whether this difference is significant could be done using a student's t-test.	We calculated the statistics again to answer **GC.2.5.** They now give identical results.	When looking at all surface stations (a), the ICO configuration exhibits a ~~slightly lower overall~~ bias that is not significantly different from the REG configuration,
SC.2.26 Figure 5: How is the data on the x-axis ordered? And why is it not ordered geographically? I would suggest sorting by latitude, so that it is easier to see whether larger differences start to occur closer to the poles.	The data was ordered by increasing standard deviation of the REG configuration for readability of the graph since there did not seem to be any link between the results and the latitude of the stations. This has been changed to be latitude-ordered as discussed in a previous comment.	

SC.2.27 Line 297: Before you can conclude that ICO better captures the gradients (growth rate?), it is necessary to add uncertainty estimates to the 1.43 and 1.3 values. Are they significantly different? If that is larger than 0.15, they are essentially the same.	We calculated the statistics again to answer **GC.2.5.** They now give identical results.	
SC.2.28 Lines 300-305: It would be very useful to see a latitude-bias plot, also as, for example, averaged data per 5- or 10-degree latitude bins, over zonal bands, to show that the bias doesn't increase significantly with latitude.	Figure 8 (new numbering) was added, containing the latitude-bias plot. It shows no major difference in the bias between the two configurations based on the latitude.	
SC.2.29 Line 307: I would use different selection criteria here for the stations shown. First, for certain sites, 8 harmonics may either be overkill or not enough. It would be justified to ignore the sites where the curve fit on observations fails to represent the data. Then, the main point of the reduced grid in the ICO has coarser resolution at the poles. If you select 1 station for every 20-degree latitude bin, you can clearly illustrate that the seasonal cycle is well captured.	As discussed in the answer to **GC.2.5**, we modified the selection criteria of stations. The new figures ordered by latitude also show that ICO captures the seasonal cycle irrespective of its coarser resolution at the poles.	

SC.2.30 Line 350: What do you mean with “variations”?	We meant to describe the general shape of the vertical profile, we reworded the sentence to be less confusing.	The vertical profiles ~~variations in vertical gradients~~ are almost identical for all altitudes
SC.2.31 Lines 375-384: What do you mean by “effective”? I am not sure if I agree with the general message in the conclusion that “it did not worsen either” or “comparable” vertical profiles. From the results section, I would say that the ICO setup gives slightly worse results, and that the only advantage is that it is somewhat faster. If computational efficiency is the most important aspect, and the slightly worse results are not an issue, one could go for ICO, but I would not see a reason to do this, since the gain is marginal. Also, as mentioned before, there is the GPU version of the same setup, and the comparison to that is missing. I wonder if with the GPU you still need the ICO configuration, since the main gain is already solved in another way.	The word “effective” was replaced with “spatial”. The ICO configuration is not only faster because of the reduced grid but provides much better scaling at high resolution, being faster and allowing a better use of computing resources. The GPU version (Chevallier et al., 2023) only refers to an offline model used for inversion of CO_2 and is therefore not comparable to the coupled models studied here. DYNAMICO can already run on GPUs when used alone and the long term development goal is to make it possible to run coupled configurations using DYNAMICO in a combined approach using GPUs for the dynamics and CPUs for the other processes. Doing this would compound the computing gains already shown in our study and is not a mutually exclusive choice. After a discussion with Bianca Baier from NOAA, we replaced our version of the Aircore dataset (from Version 20210813) by a newer version (Version 20230831). This change corrects an error in some reported altitudes. In particular, the inital data set version we used suffered from	

	issues for several flights, we switched to using the new Version 20230831 which is exempt from such issues. We corrected the description of the data used in Section 2.3 and added the correct reference where needed. This change in dataset affected the results of the comparison between our model and measurements in Section 3.5.2 and the conclusion. The different CO_2 vertical profiles between ICO and REG at high altitudes now show similar gradients and differ only in a general bias.	

Other changes

- The notation for the model DYNAMICO has been uniformized to use only uppercase letters across the manuscript.
- Following the answer to **GC.2.5** the results of the statistical analysis in Section 3.4 were modified, and the discussion of these results has been changed accordingly in that Section and in the Conclusion.
- The Figures have also been updated accordingly.
- Because of the addition of new tests at a higher resolution following several General Comments by the Reviewers, we modified the text, particularly in Section 2.1.2 and 2.2, to introduce this new resolution.
- The study from Chevallier et al. (2010) was not correctly referenced, this has been corrected.

References

[1] Agustí-Panareda, A., Diamantakis, M., Massart, S., Chevallier, F., Muñoz-Sabater, J., Barré, J., Curcoll, R., Engelen, R., Langerock, B., Law, R. M., Loh, Z., Morguí, J. A., Parrington, M., Peuch, V.-H., Ramonet, M., Roehl, C., Vermeulen, A. T., Warneke, T., and Wunch, D.: Modelling CO2 weather – why horizontal resolution matters, Atmospheric Chemistry and Physics, 19, 7347–7376, https://doi.org/10.5194/acp-19-7347-2019, 2019.

[2] Schuh, A. E., Otte, M., Lauvaux, T., and Oda, T.: Far-field biogenic and anthropogenic emissions as a dominant source of variability in local urban carbon budgets: A global high-resolution model study with

implications for satellite remote sensing, Remote Sensing of Environment, 262, 112473, https://doi.org/10.1016/j.rse.2021.112473, 2021.

[3] Zheng, T., Feng, S., Davis, K. J., Pal, S., and Morguí, J.-A.: Development and evaluation of CO_2 transport in MPAS-A v6.3, Geoscientific Model Development, 14, 3037–3066, https://doi.org/10.5194/gmd-14-3037-2021, 2021.

[4] Hourdin, F., Rio, C., Grandpeix, J.-Y., Madeleine, J.-B., Cheruy, F., Rochetin, N., Jam, A., Musat, I., Idelkadi, A., Fairhead, L., Foujols, M.-A., Mellul, L., Traore, A.-K., Dufresne, J.-L., Boucher, O., Lefebvre, M.-P., Millour, E., Vignon, E., Jouhaud, J., Diallo, F. B., Lott, F., Gastineau, G., Caubel, A., Meurdesoif, Y., and Ghattas, J.: LMDZ6A: The Atmospheric Component of the IPSL Climate Model With Improved and Better Tuned Physics, Journal of Advances in Modeling Earth Systems, 12, e2019MS001892, https://doi.org/10.1029/2019MS001892, 2020.

[5] Petersen, A. C., Spee, E. J., van Dop, H., and Hundsdorfer, W.: An evaluation and intercomparison of four new advection schemes for use in global chemistry models, Journal of Geophysical Research: Atmospheres, 103, 19253–19269, https://doi.org/10.1029/98JD01380, 1998.

[6] Quantities, Units, and Symbols in Physical Chemistry, IUPAC Green Book, 3rd edition, prepared for publication by E.R. Cohen, T. Cvitas, J.G Frey, B. Holmstrom, K. Kuchitsu, R. Marquardt, I. Mills, F. Pavese, M. Quack, J. Stohner, H. Strauss, M. Takami, and A.J. Thor, RSC Publishing [ISBN 0 85404 433 7; ISBN-13 978 0 85404 433 7], 2007

Dubos, T., Dubey, S., Tort, M., Mittal, R., Meurdesoif, Y., and Hourdin, F.: DYNAMICO-1.0, an icosahedral hydrostatic dynamical core designed for consistency and versatility, Geosci. Model Dev., 8, 3131–3150, https://doi.org/10.5194/gmd-8-3131-2015, 2015.

Remaud, M., Chevallier, F., Cozic, A., Lin, X., and Bousquet, P.: On the impact of recent developments of the LMDz atmospheric general circulation model on the simulation of CO2 transport, Geosci. Model Dev., 25, 2018.

Chevallier, F., Lloret, Z., Cozic, A., Takache, S., and Remaud, M.: Toward High‐Resolution Global Atmospheric Inverse Modeling Using Graphics Accelerators, Geophysical Research Letters, 50, e2022GL102135, https://doi.org/10.1029/2022GL102135, 2023.

Baier, B., Sweeney, C., Newberger, T., Higgs, J., Wolter, S., & NOAA Global Monitoring Laboratory. NOAA AirCore atmospheric sampling system profiles (Version 20230831) [Data set]. NOAA GML. https://doi.org/10.15138/6AV0-MY81, 2021.

ICOS RI, Bergamaschi, P., Colomb, A., De Mazière, M., Emmenegger, L., Kubistin, D., Lehner, I., Lehtinen, K., Lund Myhre, C., Marek, M., Platt, S.M., Plaß-Dülmer, C., Schmidt, M., Apadula, F., Arnold, S., Blanc, P.-E., Brunner, D., Chen, H., Chmura, L., Conil, S., Couret, C., Cristofanelli, P., Delmotte, M., Forster, G., Frumau, A., Gheusi, F., Hammer, S., Haszpra, L., Heliasz, M., Henne, S., Hoheisel, A., Kneuer, T., Laurila, T., Leskinen, A., Leuenberger, M., Levin, I., Lindauer, M., Lopez, M., Lunder, C.,

Mammarella, I., Manca, G., Manning, A., Marklund, P., Martin, D., Meinhardt, F., Müller-Williams, J., Necki, J., O'Doherty, S., Ottosson-Löfvenius, M., Philippon, C., Piacentino, S., Pitt, J., Ramonet, M., Rivas-Soriano, P., Scheeren, B., Schumacher, M., Sha, M.K., Spain, G., Steinbacher, M., Sørensen, L.L., Vermeulen, A., Vítková, G., Xueref-Remy, I., di Sarra, A., Conen, F., Kazan, V., Roulet, Y.-A., Biermann, T., Heltai, D., Hensen, A., Hermansen, O., Komínková, K., Laurent, O., Levula, J., Pichon, J.-M., Smith, P., Stanley, K., Trisolino, P., ICOS Carbon Portal, ICOS Atmosphere Thematic Centre, ICOS Flask And Calibration Laboratory, ICOS Central Radiocarbon Laboratory, 2023. European Obspack compilation of atmospheric carbon dioxide data from ICOS and non-ICOS European stations for the period 1972-2023; obspack_co2_466_GLOBALVIEWplus_v8.0_2023-04-26. https://doi.org/10.18160/CEC4-CAGK

Chau, T. T. T., Gehlen, M., and Chevallier, F.: A seamless ensemble-based reconstruction of surface ocean pCO2 and air–sea CO2 fluxes over the global coastal and open oceans, Biogeosciences, 19, 1087–1109, https://doi.org/10.5194/bg-19-1087-2022, 2022.

Jones, M. W., Andrew, R. M., Peters, G. P., Janssens-Maenhout, G., De-Gol, A. J., Ciais, P., Patra, P. K., Chevallier, F., and Le Quéré, C.: Gridded fossil CO2 emissions and related O2 combustion consistent with national inventories 1959-2018, Scientific Data, 8, https://doi.org/10.1038/s41597-020-00779-6, 2021.

Simulating the variations of carbon dioxide in the global atmosphere on the hexagonal grid of DYNAMICO coupled with the LMDZ6 model

Zoé Lloret[1], Frédéric Chevallier[1], Anne Cozic[1], Marine Remaud[1*], Yann Meurdesoif[1]

[1]Laboratoire des Sciences du Climat et de l'Environnement, LSCE/IPSL, CEA-CNRS-UVSQ, Université Paris-Saclay, Gif-sur-Yvette, France

[*] currently at Faculty of Science, A-LIFE, Vrije Universiteit Amsterdam, 1081 HV Amsterdam, the Netherlands

Correspondence to: Zoé Lloret (zoe.lloret@lsce.ipsl.fr)

Abstract. Efforts to monitor the emissions and absorptions of atmospheric carbon dioxide (CO_2) over the globe and to understand their varying regional patterns with greater accuracy have intensified in recent years. This study evaluates the performance of a new model coupling, ICO, built around the Laboratoire de Météorologie Dynamique atmospheric general circulation model (LMDZ) for simulating CO_2 transport. ICO utilizes the new icosahedral hydrostatic dynamical core called DYNAMICO~~Dynamico~~ running on an unstructured grid, which enables potential improvements in spatial resolution at the Equator while removing artificial distortions and numerical filters at the poles. Comparisons with a reference configuration using a structured latitude-longitude grid reveal that ICO well captures seasonal variations in CO_2 concentrations at surface stations. While not significantly improving the simulation~~enhancing the capture~~ of complex seasonal patterns, ICO maintains comparable accuracy. Both configurations exhibit similar vertical CO_2 concentration profiles and display a consistent bias in the lower stratosphere relative to observational data. ICO demonstrates advantages in computational efficiency and storage, thanks to its reduced cell count per level and a homogeneous grid structure. It holds promise for future developments, including with the LMDZ offline model and associated inversion system, which contribute to the Copernicus Atmosphere Monitoring Service. Overall, the ICO configuration showcases the efficacy of utilizing an unstructured grid for the physics, and the capability of DYNAMICO~~Dynamico~~ in accurately simulating CO_2 transport. This study emphasizes the importance of advanced modeling approaches and ~~high-resolution~~ innovative grids in enhancing our understanding of the global carbon cycle and refining climate models.

1 Introduction

The key role of carbon dioxide (CO_2) in climate change has motivated increasing efforts in recent decades to monitor its variations in the global atmosphere. Sources and sinks of this trace gas are found primarily on the Earth's surface. They induce the highest CO_2 gradients in the boundary layer, for example around anthropogenic emission hotspots, while their direct influences gradually mix over time at all altitudes to contribute to the overall CO_2 background. The distribution of CO_2 in the atmosphere therefore spans a wide range of spatial and temporal scales, mainly combining influences from surface sources, surface sinks and meteorology. This complexity is sampled by growing high-quality observation networks on the ground, in the atmosphere (aircraft, balloons, drones) and in space (e.g., Ciais et al., 2014; Crisp et al., 2018). It is also simulated, more or less well, by Atmospheric General Circulation Models (GCMs) and dedicated tracer transport models (e.g., Remaud et al., 2018; Basu et al., 2018; Agustì-Panareda et al., 2022). Many uncertainties in the model input data (boundary conditions, meteorology) and the model equations (advection schemes, subgrid parameterizations) still limit these simulations. However, there is a strong incentive towards higher spatial resolutions in order to benefit from an increased realism for orography, coastlines, and known

emission or absorption hot-spots, and to reduce any artificial smoothing of the 3D fields (Agustí-Panareda et al., 2019). However, this wish is tempered by the need to carry out long simulations of this long-lived tracer, typically several years, that may be massively repeated in the case of inverse modeling. Increasing the resolution without affecting the time-to-solution leads to revisiting the numerical efficiency of models in order to gain computing time margins. Porting codes on Graphical Processing Units (GPUs) may largely contribute to this effort (in particular for the simpler codes of the offline models, as shown by Chevallier et al., 2023), but not enough to close the gap between model resolution and, e.g., the kilometric resolution of the current space-borne observations. In particular, models running on a regular longitude-latitude grid face scaling limitations due to advection at the poles requiring significant data communication to solve the problem of resolution clustering. This data exchange can create a computing bottleneck on supercomputers using large amounts of processors (Staniforth & Thuburn, 2012). Moreover, the efficiency of porting existing GCMs to GPUs depends on the structure of their code, which may have to be redesigned. In this paper, we are addressing these issues for the simulation of CO_2 transport using an unstructured quasi-uniform grid made of non-quadrilateral grid cells. Such a solution is gaining popularity in recent years, either for use in Earth system models, transporting tracers or directly for atmospheric inversion (Niwa et al., 2017; Giorgetta et al., 2018; Sakaguchi et al., 2020; Zheng et al., 2021).

We build on the dynamical core DYNAMICO (Dubos et al., 2015), which has been integrated for the first time here into LMDZ, LMDZ being the GCM of the Laboratoire de Météorologie Dynamique (Hourdin et al., 2020). LMDZ has been used as the atmospheric component of the Institut Pierre-Simon-Laplace (IPSL) Earth system model (Sepulchre et al., 2020) and for the Climate Model Intercomparison Project (CMIP) with its traditional regular longitude-latitude grid. For comparisons with real observations, e.g., for inverse modeling, it is nudged to horizontal wind fields obtained from a numerical weather forecast reanalysis.

This paper evaluates the ability of this new configuration of the LMDZ GCM using the DYNAMICO dynamical core to transport a long-lived tracer like CO_2. DYNAMICO has been extensively compared to other dynamical cores (Ullrich et al., 2017) in a stand-alone fashion, but has not been evaluated yet when integrated into a GCM for use with tracer transport. Coupling DYNAMICO to the LMDZ GCM also represents the first step towards the use of DYNAMICO for inverse modeling of CO_2. We compare it to the previous reference configuration running on a regular longitude-latitude grid and to various observations of CO_2 mole fractions over a 40-year period. We also compare their computational performance at a higher resolution to judge the future scalability of this new configuration.

This study is but one stepping stone in the overall strategy of the development of the LMDZ GCM to increase spatial resolution while leveraging the advancements in high-performance computing, emphasizing manycore systems and hardware accelerators. DYNAMICO was created to meet these needs (Dubos et al., 2015) and implementing its coupling with the rest of the GCM as well as validating its performance against a reference configuration for tracer transport are pivotal steps in this development. Analyzing the computational performance of this new configuration and its scalability will also help inform decisions on future porting of these models and coupled configurations to GPUs.

Section 2 describes the two configurations of our GCM, the developments done to create our new configuration, the experiments we ran to compare them, and the method for our study. Section 3 presents a performance comparison of our configurations and the results of the direct comparison between our models and the observations. Section 4 concludes the study.

2 Presentation of the model and experiments

2.1 Configuration~~Model~~ description

~~2.1.1 LMDZORINCA - Regular longitude-latitude configuration~~

In this study, we compare two configurations of the LMDZ GCM that each couple different individual models. The full configurations are schematized in Figure 1. The individual models are presented in section 2.1.1 and the newly developed configuration is presented in detail in section 2.1.2.

Our reference general circulation model configuration (Fig. 1) consists of the coupling between the LMDZ model of Hourdin et al. (2013, 2020) itself, an aerosol and reactive chemistry model called INteractions between Chemistry and Aerosols (INCA, Hauglustaine, et al., 2004) and the Organizing Carbon and Hydrology in Dynamic Ecosystems land surface model (ORCHIDEE, Krinner et al., 2005). ORCHIDEE simulates the water and energy exchanges between the soil and the atmosphere, but yearly land cover maps were used here instead of simulating vegetation dynamics. In the following, we will refer to this LMDZ-INCA-ORCHIDEE coupled model on the regular latitude-longitude grid as REG for simplicity.

We have developed a novel configuration that couples the ORCHIDEE land surface model, the INCA chemistry model, and the physics module of the LMDZ model. The previous dynamical core in LMDZ has been replaced by a new one, known as DYNAMICO (Dubos et al., 2015), which operates on a quasi-uniform icosahedral C-grid for its horizontal mesh (Fig. 1). In the following, we will refer to this DYNAMICO-LMDZ-INCA-ORCHIDEE coupled model as ICO for simplicity.

Both configurations use XIOS, a tool that allows asynchronous and parallel input and output of files.

Each of these pre-existing models can be operated either independently using precomputed files as input, or using information from other models to which they are coupled. We will describe them and their role in our configurations in the following subsection.

3

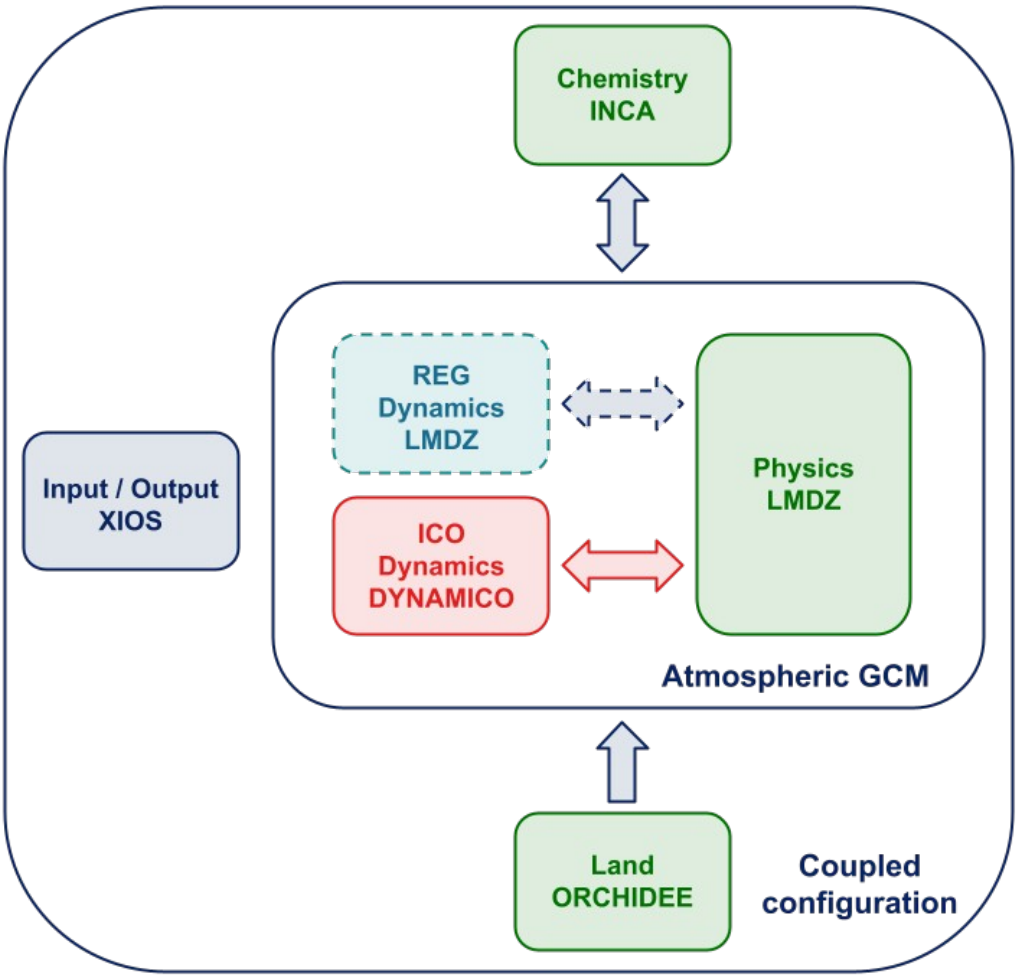

Figure 1: The structure of the two coupled configurations REG and ICO. Both use the same models for the physics, land surface and chemistry but they each use a different dynamical core. For the ICO configuration, the new coupler between DYNAMICO and LMDZ as well as XIOS ensure a seamless transition with the new icosahedral grid for all the models.

2.1.1 General description of the two models

The two configurations use the same individual physics, land and chemistry models but use different dynamical cores.

In our configurations, ~~T~~tracers, such as CO_2, are outputted~~modeled~~ by INCA, and their transport is calculated and synced with the LMDZ GCM physics time step ~~every 15 minutes~~. Chemical processes are also calculated at this same frequency~~every 15 minutes~~ by computing differential equations to update the atmospheric mole fraction~~concentration~~ fields of each cell. Using tracers from INCA instead of only having them in LMDZ allows interaction between chemical reactions and the tracer transport process, which is crucial for some tracers such as CH_4, although it has no impact on CO_2. In our study, these chemical processes are not applied to the CO_2 tracer.

The latest version of LMDZ physics is described in Hourdin et al. (2020). Most notably for tracer transport, dry and cloudy shallow convection is separated from deep convection. Shallow convection is unified and combines the Mellor and Yamada (1974) diffusive approach for small-scale turbulence with a thermal plume model (Rio & Hourdin, 2008) for the boundary layer. Deep convection uses a modified version of the mass-flux formulation of Emanuel (1991) (Grandpeix et al., 2004, Rochetin et al., 2014). Longwave radiation is modeled using the Rapid Radiation Transfer Model (RRTM; Mlawer et al., 1997), and shortwave radiation uses a 6-band code derived from Fouquart and Bonnel (1980).

4

The dynamical core of LMDZ discretizesis a mix of a finite-difference and finite-volume discretization on the sphere of the primitive equations of meteorology and of transport equations (Hourdin et al., 2006, 2013). Water and other tracers are advected with a scheme from Van Leer (1997), and angular momentum is conserved numerically. This full configuration was previously evaluated for CO_2 transport by Remaud et al. (2018).

The dynamical core of LMDZ is parallelized in latitude using distributed memory with the Message Passing Interface standard (MPI) and in the vertical with shared memory using the Open Multi-Processing interface (OpenMP). A longitudinal filter near the poles avoids the use of very small time steps, but limits the efficiency of any parallelism along the longitudes.

The parallelization of the physical parameterizations within LMDZ follows a different approach. It utilizes a combination of MPI and OpenMP processes with shared memory by splitting a single vector that runs through the entire horizontal grid into independent domains. This is possible due to the fundamental 1-D nature of the LMDZ physical parameterizations that only compute vertical transfers. The performance of the model is optimized by using domain decomposition parallelism on the horizontal layer with MPI and shared memory parallelism with OpenMP.For LMDZ at our resolution , the optimal compromise between resources and performance is achieved by using 71 MPI processes with 8 OpenMP threads running on 568 cores (Hourdin, 2020).

2.1.2 ICOLMDZORINCA - unstructured grid configuration

ICOLMDZORINCA is a novel configuration of our coupled model that integrates the previously described ORCHIDEE land surface model, the INCA chemistry model, and the physics module of the LMDZ model. The previous dynamical core in LMDZ has been replaced by a new one, known as DYNAMICO (Dubos et al., 2015), which operates on a quasi-uniform icosahedral C-grid for its horizontal mesh. In the following, we will refer to this DYNAMICO-LMDZ-INCA-ORCHIDEE coupled model as ICO for simplicity.

DYNAMICO is a dynamical core that can solves Tthe hydrostatic and shallow-atmosphere non-hydrostatic Euler equations can be solved using the DYNAMICO dynamical core (Ullrich et al., 2017). In this study, the hydrostatic mode was used. The mesh is based on a tessellation of the sphere into triangles, which when joined, creates the primal hexagonal-pentagonal mesh. A quasi-uniform grid avoids any singularity at the poles, thereby improving the load balancing on parallel computers. By construction, this grid has a coarser spatial resolution than a regular longitude-latitude grid in the high latitudes, even when accounting for the longitudinal polar filter (Herrington et al., 2022preprint). The cells have similar areas across the globe, from the equator to the poles, unlike in the regular longitude-latitude grid where cell size gets systematically smaller when approaching the poles. Figure 21 provides an example of a visual representation of the icosahedral C-grid.

Kinematics and dynamics were separated as much as possible so that transport equations do not use any information from the momentum equations. The kinematics handle the transport of mass, potential temperatures, and tracers using the mass fluxes computed by the dynamics. The vertical transport uses a slope-limited Van Leer's scheme (Van Leer, 1977) and does not differ from the REG configurationvertical transport of LMDZ. The fully discrete finite volume horizontal advection scheme is described in Dubey et al. (2015). It uses a flux-corrected transport approach to stay positive-definite rather than slope limiters.

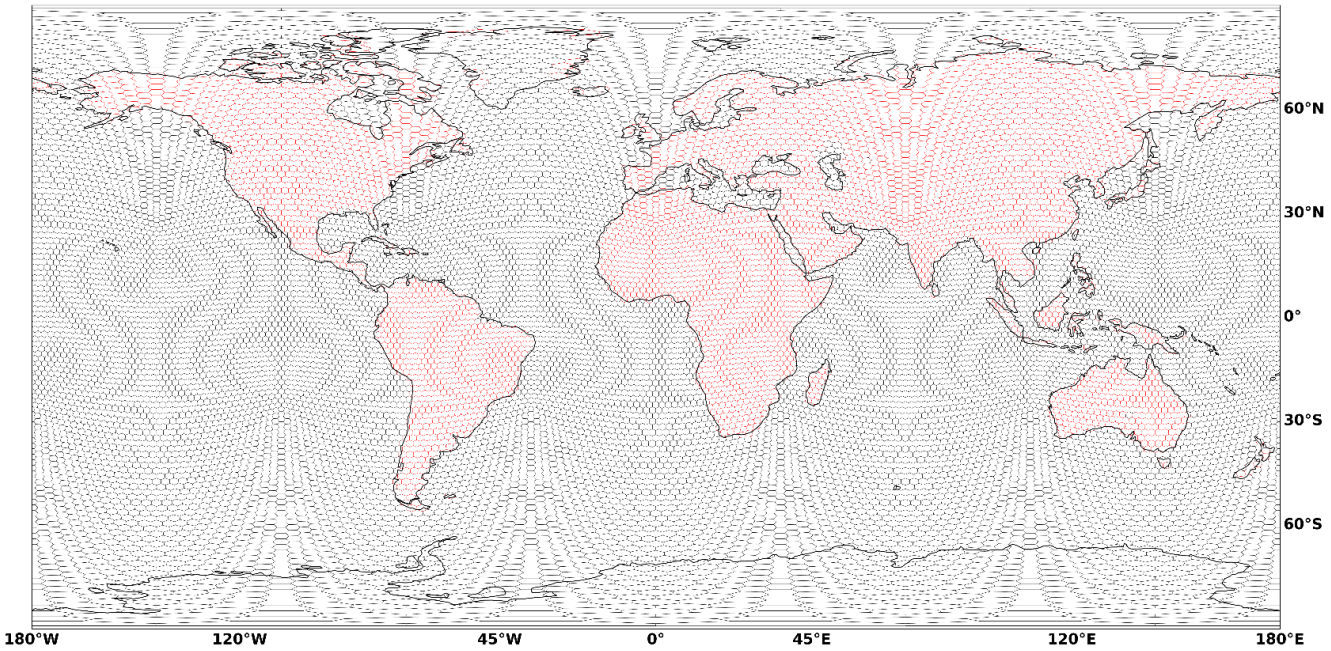

Figure 2: Icosahedral grid of the ICO configuration with with a horizontal grid of 16002 cells (see section 2.2 for a description of the resolution).

2.1.2 ICO - New icosahedral grid configuration

DYNAMICO, the dynamical core itself of this new configuration, was already developed and presented in Dubos et al. (2015) but not coupled with the physics of LMDZ at the time, nor used as part of a larger coupled configuration with a chemistry or land model. To that goal, a specific module handling the coupling of the dynamical core to the physics of LMDZ was needed.

This coupler specifically interfaces the dynamics with the already existing physics of LMDZ, with an asynchronous time step. The time step of the dynamics is inextricably linked to the resolution of the model. **For** ~~lower~~ the main **resolution** ~~like the ones,~~ **used in this study** and described in section 2.2**, the dynamics time step is 7.5 minutes, half that of the physics and identical to the time step in the REG configuration. This time-step has to be reduced accordingly when increasing the resolution** in Section 3.2 **to satisfy convergence conditions. Another important part of this coupler is interpolating the interfaced variables since some variables in the dynamics are computed at the edges or vertices, whereas the physics uses centered variables.**

The global mesh used in the ICO configuration is partitioned into 10 quadrilateral clusters of similar size to map the sphere. Each quadrilateral is paved with the same number of hexagonal cells, depending on the chosen resolution. It can be subdivided along two directions, i and j, thus generating sub-tiles in the form of parallelograms composed of $iim \times jjm$ hexagons (Fig. 3).

6

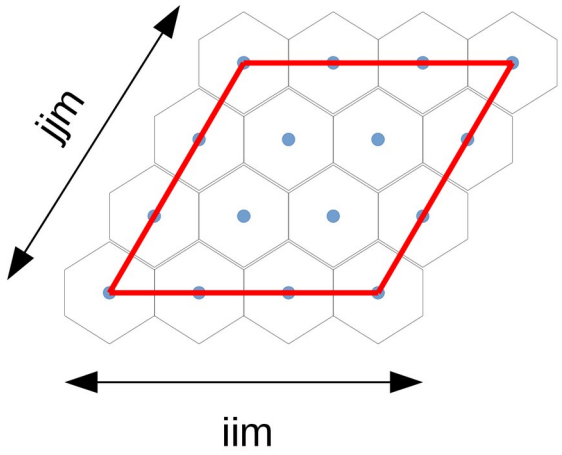

Figure 3: Subdivision of the primary mesh quadrilateral along the two directions i and j.

MPI parallelism is achieved by distributing the sub-tiles thus created to each MPI process, the optimum performance being achieved for sub-tiles of identical size and with only one sub-tile per MPI process. When solving the various numerical schemes of the dynamic core, the data required at the domain boundaries is transferred by asynchronous MPI calls from one sub-tile to another. OpenMP parallelism operates through shared memory, distributing computational iterations on vertical levels over threads created within an MPI process, in a similar fashion to the REG configuration.

~~To achieve efficient parallelism in the horizontal dimension, the ICO configuration partitions the mesh into rhombi, whose sides pass through the centers of some of the hexagons. The hexagons covered by a rhombus are processed together and the rhombi can be processed in parallel. This parallelization strategy is implemented with a combination of OpenMP and MPI.~~

~~The vertical parallelization is identical to the one in the REG configuration.~~

Tracer storage was handled very differently between DYNAMICO and LMDZ and had to be uniformized. Initially, DYNAMICO tracers were only identified by a unique number and handling them necessitated always knowing which tracer corresponded to which index number in the tracer variable defined in a unique tracer definition file. LMDZ on the other hand was able to dynamically access tracers identified by chemical species or isotope name. Definition and initialization of tracers is now unified through a single file, and a parser was created so that tracers in DYNAMICO can be linked to these same chemical species names.

Another important feature that had to be developed was the ability to nudge the atmospheric GCM to variables such as winds, temperature or surface pressure. This feature was already available in the REG configuration but had to be re-created for the ICO configuration. A new guided mode was added to the dynamical core DYNAMICO, and special care had to be taken to keep the ability to nudge the variables either at a global scale or restricted to certain areas only of the icosahedral grid. Such restrictions are often parametrized in latitude-longitude coordinates and must be properly interpolated to the icosahedral grid while handling the conditions at the edge of the nudged area. This development is also essential for future use of the DYNAMICO - LMDZ coupling as a limited-area model.

7

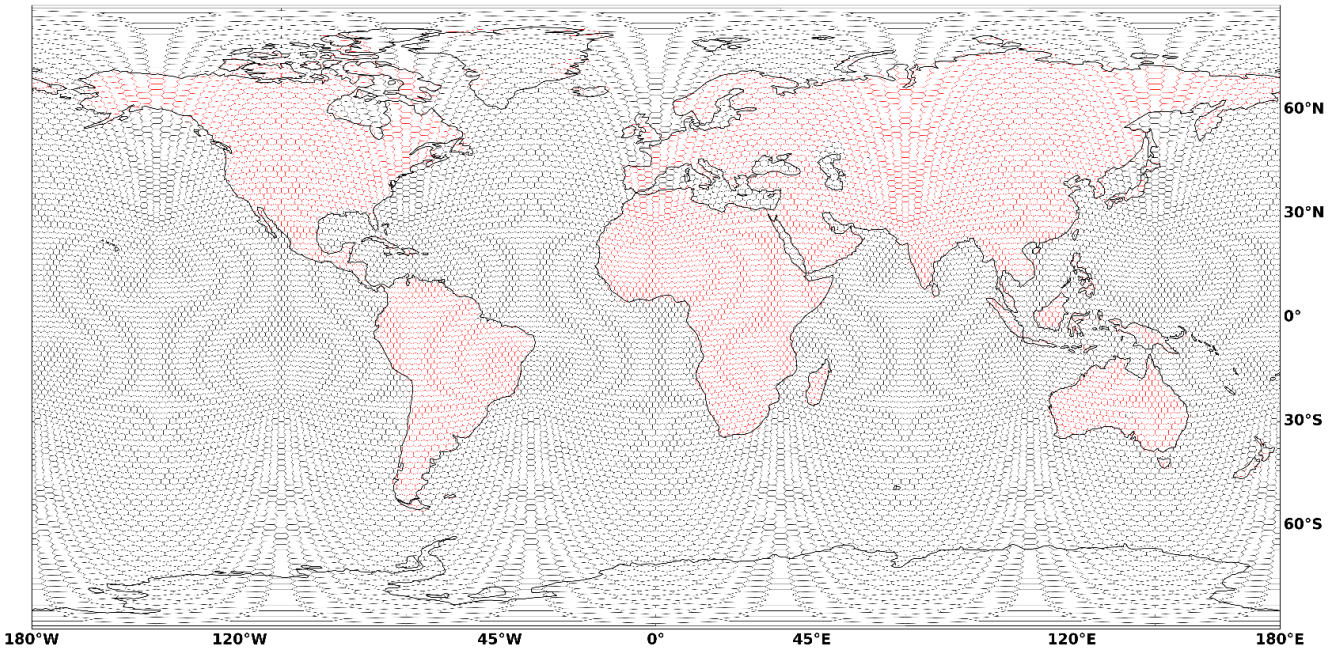

~~Figure 1: Unstructured grid of the ICO configuration used here.~~

2.2 Description of the simulations

For each configuration (REG and ICO), we have run a simulation from 1979 to 2020. The first year is used for spin-up and is not analyzed. In both configurations, the large-scale atmospheric circulation was nudged to the 6-hourly horizontal winds from the ERA5 reanalysis~~In both configurations, the model was not let free, but its large-scale atmospheric circulation was kept in the vicinity of the observed one by nudging its 6-hourly horizontal winds toward the ERA5 reanalysis~~ (Hersbach et al., 2020) with a relaxation time of 3 hours. The nudging drives the large-scale atmospheric circulation of the model. Initial atmospheric CO_2 mole fractions~~mixing ratios~~ values were set using the Copernicus Atmosphere Monitoring Service (CAMS) atmospheric inversion, version 20r2 (Chevallier et al., 2005; https://atmosphere.copernicus.eu/, access 31 May 2023). This same product prescribed the CO_2 surface fluxes every 3 hours. Prior fluxes used for this product were GCP-GridFED version 2021.2 for anthropogenic emissions (Jones et al., 2021), GFED 4.1 inventories for biomass burning, ocean fluxes from Chau et al. (2022) and climatological biosphere-atmosphere fluxes from an ORCHIDEE simulation, version 4.6.9.5.

These surface fluxes carry some imprint from the REG model with a regular grid, since the CAMS database used~~s~~ an older REG model version at coarser spatial resolution. Still, after Remaud et al. (2018) who tested a distinct set of surface fluxes for their model evaluation within a similar framework, we consider that this imprint hardly affects our conclusions.

The boundary files used for the two simulations were identical (aerosol, oxydants and ozone mole fraction, solar forcing, land use maps). However, for the simulation running on ICO, the boundary files were either interpolated or recreated onto the new grid ahead of time to fit the unstructured grid or interpolated during execution. The initial total mass of CO_2 in the atmosphere had a difference of only 0.01% between the two simulations because of these operations.

We had an hourly model output for all variables. This high frequency output was chosen in order to well assess the differences in synoptic variability of tracer transport between our two model configurations.

8

We used two different horizontal resolutions in this study, the lower resolution one was used in our main simulations to compare the difference in CO_2 tracer transport between our two configurations. We chose this resolution because it was an already established and studied resolution for our reference REG configuration, allowing us to study only the influence of the new dynamical core and grid. We also performed computational performance tests at a high resolution to test the scaling of our two configurations and make better informed decisions about their future development.

For our main simulation, ~~W~~we ran REG on a horizontal grid of 144 points in longitude × 143 grid points in latitude, which corresponds to a resolution of 2.5° in longitude and 1.27° in latitude, equivalent to 278 km by 140 km at the equator. We use 79 vertical layers going up to 80 km in altitude, with around 25 layers dedicated to the first 2 km. The complete grid configuration is described in more detail in Hourdin et al. (2020).

We compared this configuration with ~~We ran~~ ICO running on a horizontal grid of 16002 cells, and the same 79 vertical layers. This gives an horizontal resolution at the equator of around 2.5° in longitude and 1.25° in latitude, each cell has the area of an hexagon of side 110 km in order to have similar resolution at the equator to the equivalent longitude-latitude grid from REG. With this setup, ICO has 22% less cells than REG.

For the performance tests of the configurations running at a higher resolution, REG has an horizontal grid of 256 points in longitude × 256 grid points in latitude, which corresponds to a resolution of 1.4° in longitude and 0.7° in latitude, equivalent to 157 km by 78 km at the equator. In this test, ICO was run on an horizontal grid of 64002 cells,, with hexagons of side 55 km. Both configurations still have 79 vertical layers and at this higher resolution ICO only has only 2% less cells in total than REG but with a higher spatial horizontal resolution.

2.3 Observational data

To compare our simulated tracer mole fraction~~concentration~~s to observations, we sampled the mole fraction~~concentration~~ fields at the nearest cell center, model level and timestamp for each data point. We used the high-quality measurements of the CO_2 GLOBALVIEWplus v8.0_2022-08-27 ObsPack database (Schuldt et al., 2022, Miles et al., 2017, Miles et al., 2018, ICOS RI, et al., 2023, Lan et al., 2023). For AirCore, we used the dataset from NOAA Version 20230831 (Baier et al., 2021).

In this dataset, observations were calibrated according to the WMO CO_2 X2019 scale (Hall et al., 2021). Like for inverse modeling with LMDZ (Chevallier et al., 2010), only afternoon non flagged data from 12:00 to 16:00 local time were selected for continuous in-situ surface stations under 1000 m above sea level (a.s.l.), and only night time data from 00:00 to 4:00 local time were kept for in-situ stations above 1000 m a.s.l. ~~All flask data, and all upper-air data (aircraft data and AirCore measurements) were kept.~~ This selection accounts for the usual failure of transport models to well represent the accumulation of tracers at low altitude during the night as well as the inability to model the phenomenon in mountain stations where air masses are advected during daytime through updrafts on the sun-exposed slopes (Geels et al., 2007). All flask data, and all upper-air data (aircraft data and AirCore measurements) were kept.

We divided the observations into three groups: surface in situ and flask data, aircraft observations and observations from AirCore flights. We used the aircraft measurements and AirCore data to obtain vertical profiles of CO_2 mole fraction~~concentration~~. ~~AirCore (Karion et al. 2010) is an atmospheric sampling system consisting of an open ended steel tube launched from an aerial platform and that collects many successive samples of the ambient air when descending.~~ For surface data, 10~~7~~6 stations have been selected from the Obspack dataset out of the original 222 stations. Surface stations with less than 5000 measurement points

9

that passed the initial data selection described above over the entire duration of the study were excluded from the analysis. For aircrafts, we have selected 33 sites and campaigns out of a possible 51, only keeping those with more than 2000 measurement points. For the AirCore data, we kept all observations. The full list of sites and datasets used is presented in Table 1 and Table 2 as a supplement.

The uncertainty of the reference CO_2 mole fraction~~mixing ratio~~ measurements used here is on the order of 0.1 ppm (see, e.g., Crotwell et al., 2020, for the systematic errors and Hazan et al., 2016, for the standard deviation). It is negligible compared to the model uncertainty due to transport error which is on the order of 1 ppm under 3000 m (Lauvaux et al., 2009) and is not further discussed in the following. Collection altitude determination error from AirCore measurements can be high and depends on the altitude, and is on the order of 250 m below 20 km and up to 1 km above that altitude (Wagenhäuser et al., 2021). ~~We discuss the potential impact of these uncertainties on our model evaluation in section 3.5.2.~~

2.4 Evaluation methodology

2.4.1 Surface stations

For surface stations with continuous measurements, we used a curve-fitting method using a non-linear least squares method on both the model and observations CO_2 mole fractions~~mixing ratios~~ time series to extract the annual mean, the seasonal cycles and the synoptic variations. A smoothed function consisting of a second-order polynomial and eight harmonics was used to fit the time series over the 19~~0~~80-2020 period (equation 1). We excluded stations where the fit of the measurements had a coefficient of determination under 0.75, for a total of 85 stations. The polynomials were used to calculate the annual trend and growth rate, while the harmonics were used to get the seasonal cycle. ~~The synoptic variations are obtained from the difference between the raw data~~ (~~and the fitted smooth curve~~ (equation 2)~~.~~

$$f(t) = p_1 \cdot t + p_2 \cdot t^2 + \sum_{k=3}^{10} p_k \cdot \sin(2\pi k t) \quad (1)$$

$$r(t) = x(t) - f(t) \quad (2)$$

Equation 1 corresponds to the fitted function of CO_2 mole fractions f with t being the time. The different parameters p_k are coefficients fitted after optimization and unique to each model and station. The parameters up to p_2 correspond to the general trend of the growth rate of atmospheric CO_2, and the parameters of the sinusoidal function to the seasonal cycle. The residual, corresponding to the synoptic variations, r, are obtained from the difference between the raw measured or modeled CO_2 mole fraction x and the fitted smooth curve f (Equation 2).

To evaluate the two model configurations performance between each other and compared to observations we use metrics which we will describe in the following subsections.

2.4.2 Annual gradient between stations

We use the measurements from South Pole station (SPO), which is far from any major CO_2 source or sink, to validate the simulated background growth rate of CO_2 mole fraction~~concentrations~~. Then, we study the cross-site gradients by calculating the yearly growth rate at each site relative to SPO. To do so, we average the annual growth rate of the CO_2 mole fraction~~concentration~~ over the 1980-2020 period for each site and subtract the value at SPO. Comparing the observed and modeled values of this variable informs us on both the growth rate of the CO_2 mole fraction~~concentration~~ at each site, and on mole fraction~~concentration~~ gradients of our transport model which are key for use in an inverse system. To study the interannual variation of these growth rates, we calculate their standard deviation for both measurements and models. We normalize the average model's standard deviation by dividing it by the measurement standard deviation. This gives us information on how well

10

the model captures the magnitude and direction of these variations.

We compute the yearly growth rate for each year of the 1980-2020 period using the smooth curved fit described above, before averaging it. To evaluate this variable, we then look at the mean bias and the root-mean-square error (RMSE) of the CO_2 mole fraction~~concentration~~ gradient for each station relative to SPO.

2.4.3 Seasonal cycle

We evaluate the capacity of our model to represent the CO_2 seasonal cycle by comparing the phase and amplitude of the harmonics of their smoothed fitted curve to the one of the measurements at each station. At each measurement site we calculated the Pearson correlation coefficient between measurements and model time series to evaluate the phase of the seasonal cycle. And we evaluated the amplitude of the seasonal cycle by looking at the ratio between peak-to-peak amplitudes of the harmonics. We normalized this variable by dividing the values of the model's seasonal cycle peak-to-peak amplitude at each station by the ones from the observations.

2.4.4 Synoptic variability

To evaluate our model ability to represent the phase of the CO_2 synoptic variability we again used the Pearson correlation coefficient between the residual from the smoothed fitted curve of the model and the measurements. The amplitude of the synoptic variations at each station were evaluated by the normalized standard deviation.

2.4.5 ERA5

To compare the simulated temperature with the ERA5 reanalysis, we divided the output into seasons and then into bins of 30° latitudes. For each bin, we averaged the data for each model level for each season. We then did an identical operation on the ERA5 reanalysis data before comparing the two.

2.4.6 Aircraft measurements

The aircraft measurements have been binned into 1 km altitude bins, and then averaged for each hour and over each bin for each site or campaign. Then the data was averaged over all sites and campaigns. This process was done for each season and for the whole year.

2.4.7 AirCore measurements

For measurements from AirCore, we binned and averaged the data into 50 altitude bins, from the ground to the maximum altitude of the data (27 km) to get an average vertical profile of CO_2 mole fraction~~concentration~~s.

3 Results and discussions

3.1 Mass conservation

Conservation of mass is closely examined for the simulation of long-lived tracers as it directly supports the simulation of the tracer's global growth rate. In inverse systems, it makes it possible to infer surface fluxes far from observations, far in space as well as in time. In practice, numerical approximations may make the model lose or gain tracer mass (Houweling et al., 2010).

In this section, we evaluate mass conservation in our models by calculating the total mass of atmospheric CO_2 at the beginning and at the end of the simulations. ~~To do that, we multiply the CO_2 mole fraction with the air mass in each cell and sum it over the whole globe. We then compare the difference between the CO_2 mass at the end and beginning with the total amount of prescribed~~

11

surface CO_2 fluxes. The difference between these two values is the amount of CO_2 lost or gained by our model over time.

$$\Delta m_{(CO_2)} = m^{e}_{(CO_2)} - m^{i}_{(CO_2)} = \sum_{n=1}^{Ncell} m^{n,e}_{air} \times w^{n,e}_{(CO_2)} - \sum_{n=1}^{Ncell} m^{n,i}_{air} \times w^{n,i}_{(CO_2)} \quad (13)$$

$$m^{emi}_{(CO_2)} = \sum_{t=1,n=1}^{T,N} q^{t,n}_{(CO_2)} \times A^{n} \quad (42)$$

$$m_{loss} = m^{emi}_{(CO_2)} - \Delta m_{(CO_2)} \quad (53)$$

To do that, we calculate *Δm, the observed increase in the total amount of atmospheric CO_2 over a certain period of time. In Equation (1), superscript e corresponds to the end time step of a given period studied, and i is the initial time step. We multiply the CO_2 mass fraction* w *with the dry air mass* m_{air} *in each cell and sum it over the whole grid (*N cells*).*

We then separately calculate the total emitted mass of CO_2 over a period of time, $m^{emi}_{(CO_2)}$ *in Equation 4, by multiplying the surface fluxes q with the area of each cell* A^{n} *and summing it over time.*

The difference between these two values, m_{loss} *in equation 3, is the total mass of atmospheric CO_2 lost or gained by our model over a certain period of time.*

For REG, the difference is equal to -0.13 % of the CO_2 mass emitted over the 1979 - 2020 period. For ICO it is -0.28 % for this same period.

Therefore, while our models do not exactly conserve mass, they lose only around 0.014 GtC integrated over 10 years for REG, and 0.027 GtC for ICO.

The total amount of CO_2 in each model also depends on the prescribed surface CO_2 fluxes described in section 2.2 ($m^{emi}_{(CO_2)}$) which are interpolated on the 2 different grids and therefore, not strictly identical either for each configuration. However, the average difference in yearly emitted CO_2 between the two model configurations is 0.0006 % only.

We verified that the routines in the LMDZ physics and in the dynamical cores of both configurations perfectly conserved mass. Therefore, the small mass difference comes from discrepancies between the time-integrated values of emissions and mole fractions of our tracer, but we did not investigate it further given its negligible impact in our study.

3.2 Computational efficiency

3.2.1 Computational setup

Simulations were run on the Skylake partition of the Joliot Curie, a BullSequana X1000 supercomputer operated since 2017 by Très Grand Centre de Calcul (TGCC, Bruyère-le-Châtel, France). This partition is composed of 1656 nodes, each of which has an Intel Skylake 8168 dual-processor. We used the Intel Fortran compiler version 20.0.0.

For our main simulations (called “Production run” in Table 1), REG used 47 MPI processes and 8 OpenMP threads for a total of 384 Central Processing Unit (CPU) cores, while ICO employed 80 MPI processes and 4 OpenMP threads for a total of 336 CPU cores (Table 1). This choice was made as a compromise between fast time-to-solution for the simulations, and small number of nodes for lower queue time. On average, over the whole simulation, REG achieved a wall-clock-time of 2594 seconds and consumed 2767 CPU hours per month simulated, while ICO executed in 2238 seconds and consumed 2089 CPU hours per month simulated. These results indicate that ICO provides a speedup of 14% in total CPU hours consumed over REG, with 22%

12

~~less cells.~~ This "Production run" is made with an hourly output for 26 physical and tracer variables to have a precise understanding of the CO_2 tracer transport dynamics. This output frequency significantly increases the execution time and would generally be lower for most routine use of this configuration.

~~These results n our case outputting large amounts of variables every hour greatly increases the execution time and becomes a computational bottleneckI, i. are highly dependent on the given output frequency of our simulation.~~

To better compare the configurations scaled up and in their ideal state, speed tests were run with different numbers of CPUs and ~~identical numbers of CPUs: 71 MPI processes and 8 OpenMP threads~~ with ~~an~~ additional ~~8~~ CPUs used for XIOS servers ~~for a total of 576 CPU cores~~. XIOS is a tool used for reading the input files in parallel and we chose 8 servers to ensure that this operation does not become a computational bottleneck for our models. Only monitoring files tracking the progress of the simulations were output, no physical variables were saved in order to avoid comparing the time it takes to write the files on disk. To avoid variability due to individual node performance, the tests were performed multiple times over several days, and outlier months caused by node performance issues were removed. In addition, we used timers in the code to evaluate what percentage of the time is spent in the routines of the physics versus the dynamics.

The first experiment (called REG/ICO-Speed test in Table 1) consisted in using identical numbers of CPUs for both configurations, running at the same resolution as our main simulations: 71 MPI processes and 8 OpenMP threads. Another experiment (ICO-Optimal scale) was run using 160 MPI processes and 4 OpenMP threads, more suited for the parallelization scheme of the ICO configuration. ~~The average monthly time to completion in this setup for REG was 823 seconds (132 CPU hours), and for ICO 662 seconds (106 total CPU hours). This shows that for identical computational setups~~ ~~This speedup is comparable to the reduced number of cells in ICO. For our spatial resolution, it seems that other differences such as the absence of a polar filter for ICO did not significantly improve the computational speed.~~

To test the scaling potential of the new ICO configuration at a higher horizontal resolution (HR) compared to REG, similar speed tests were run for each configuration at high resolution at two different scales. The first test was run with a small amount of CPU cores (called Low-scale in Table 1) using the same optimal number of MPI processes and OpenMP threads as the lower resolution one. A second test was run with more CPUs (called High-scale in Table 1), optimized for this higher resolution. For REG, this meant using 128 MPI processes and 8 OpenMP threads. For ICO, using 640 MPI processes and 4 OpenMP threads.

Simulation	Total CPU cores	MPI processes	OpenMP threads	Average monthly CPU (hours)	Monthly time to solution (seconds)	Time spent in dynamics (%)	Time spent in physics (%)
REG-Production	384	47	8	277	2594		
ICO-Production	336	80	4	209	2238		
REG-Speed test	576	71	8	132	823		
ICO-Speed test	576	71	8	106	662		
ICO-Optimal scale	640	160	4	63	357	15	75
REG-HR-Low-scale	576	71	8	132	829	42	54
REG-HR-High-scale	1024	128	8	237	832	33	60

ICO-HR-Low-scale	640	160	4	125	702	30	64
ICO-HR-High-scale	2560	640	4	230	323	35	55

Table 1: Computational setup and results of the simulations. The total number of CPU cores used in each simulation may be higher than the product of MPI processes by OpenMP threads since **entire nodes were reserved for better memory efficiency even though not all of their CPUs were needed**.

3.2.2 Computational gains

For our production runs, on average, over the whole simulation, REG achieved a wall-clock-time of 2594 seconds and consumed 277 CPU hours per month simulated, while ICO executed in 2238 seconds and consumed 209 CPU hours per month simulated (REG-Production and ICO-Production in Table 1): in this case, ICO consumes 25% less CPU hours compared to REG, with 22% less cells. Most of the gains for this setup with heavy output levels could therefore be attributed to the reduced grid size.

The average monthly time to completion for the first speed test for REG was 823 seconds (132 CPU hours, REG-Speed test in Table 1), and for ICO 662 seconds (106 total CPU hours, ICO-Speed test in Table 1). This shows that for identical computational setups at this reference resolution, ICO is on average 20% faster than REG. This is again only of the order of the reduced grid size, showing that in this setup, other differences such as the absence of a longitudinal ~~polar~~ filter did not significantly improve the computational speed.

The ICO gain was increased by optimizing the distribution of MPI processes and OpenMP threads to better fit the parallelization scheme of ICO (ICO-Optimal scale in Table 1). In this optimized setup, ICO consumes 52% less CPU hours than the REG configuration, a gain in computing ressources much greater than the one only due to the reduced grid size. This highlights the importance in optimizing the computing resources to each configuration for better performance.

At the high resolution (REG-HR-Low-scale, REG-HR-High-scale, ICO-HR-Low-scale and ICO-HR-High-scale in Table 1), ICO only has 2% less total cells than REG but is still faster. More importantly, it scales much better than the REG configuration, with the monthly time-to-solution going as low as 323 seconds when using 2560 CPUs. This is not the case for the REG configuration which plateaus at around 830 seconds per month irrespective of the increase in number of used CPUs. Further scaling is impossible for the REG configuration since it needs at least two latitude bands per MPI process, which means that 128 is the maximum number of MPI processes possible for this resolution.

This shows that while performance gains were modest in our main simulation, and only of the same order as the reduction in grid size, the performance gain increases when resolution increases or computing resources scale up. This gives a strong incentive to use an icosahedral grid compared to a regular latitude-longitude grid for future high-resolution studies using the LMDZ GCM.

3.3 Vertical temperature profiles

To get a first idea of the differences between REG and ICO simulations, we consider atmospheric temperature and compare it with ERA5 values. Note that our models are nudged toward ERA5 horizontal winds (Section 2.2), but do not use the ERA5 temperature fields. Figure 4~~2~~ shows the vertical profiles of the average temperature over the year 2000 for different zonal cuts in 60° latitude increments. We can already see that REG and ICO differ on several aspects for different altitudes. The tropopause height, as identified by the change in the vertical temperature gradient, is the same in both configurations, but its temperature varies between 2.5 K to 5 K for each configuration outside of the tropics. At the stratopause, a difference of up to 10 K for the yearly temperature average in high latitudes is observed between the simulations from REG and ICO (Not shown on the figure).

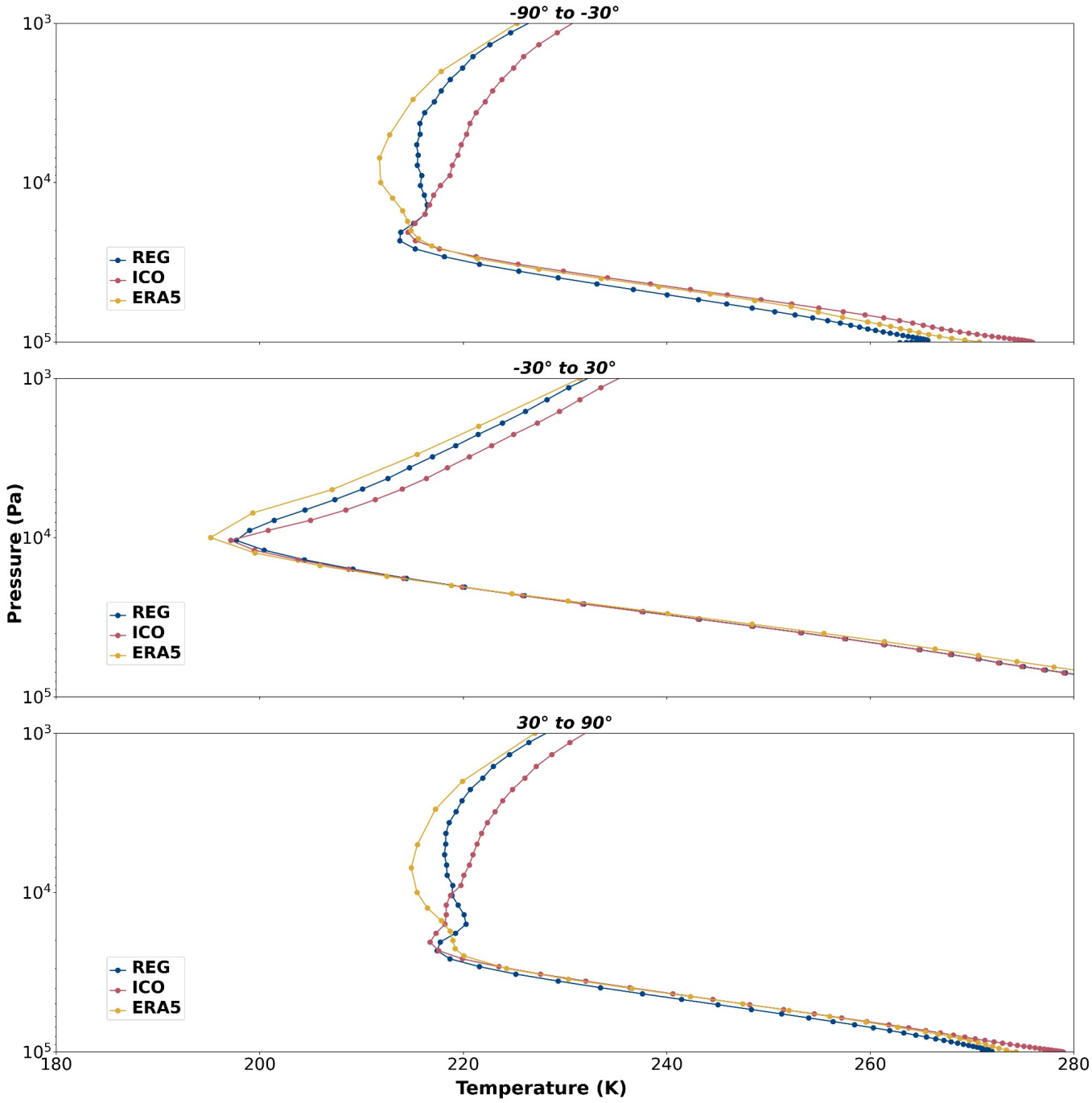

Figure 42: Vertical profile of zonal temperatures averaged over the year 2000 for the two model configurations and the ERA5 reanalysis, with REG in blue, ICO in red and ERA5 in yellow.

Looking at the temporal change of the temperature rather than yearly averages reveals a different pattern. We can see on Fig. 53 that the large temperature difference at the stratopause between our configurations is only present during winters for high latitudes. During summers, both configurations have much more similar temperatures in these latitudes, and all year around in the tropics. This is explained by the fact that during summers, the polar stratopause is mainly driven by ozone, whereas in winter it is driven by gravity-waves (Hitchman et al., 1989). The difference in parametrization and tuning of gravity waves in DYNAMICO used in our new configuration ICO compared to the previously used and much-tested REG version likely explains the observed differences in temperature of the stratopause. This large difference in temperature in the stratosphere also affects temperature lower in the troposphere, as has been shown for the stratospheric dynamics of the LMDZ GCM in Lott et al. (2005).

15

Future versions of the ICO configuration will contain a better parametrization of gravity waves as well as the introduction of a so-called “sponge layer” (Shepherd et al., 1996) to nudge high atmospheric winds towards zonal averages, which was already present in the REG configuration but not in ICO yet.

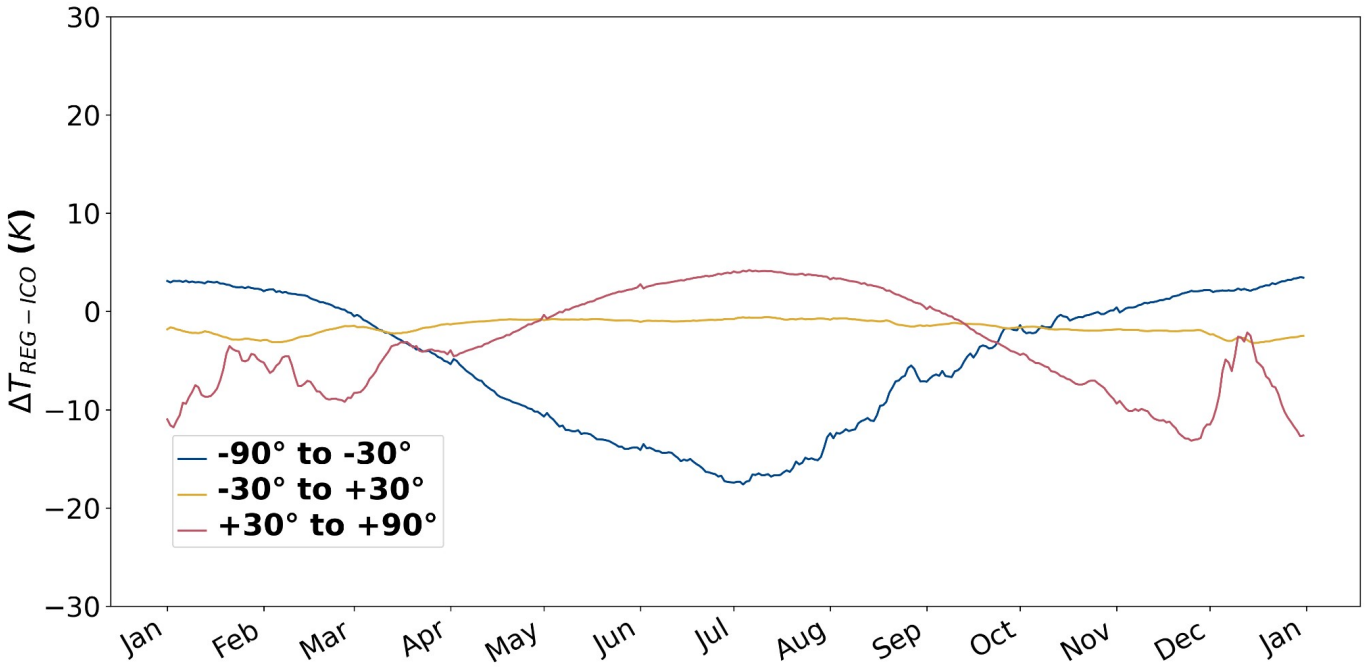

Figure 53: Time series of the average difference in zonal temperature at the stratopause (53 km) between the two model configurations REG and ICO for the year 2000, divided in 3 latitude zones of 60°.

We now turn to CO_2 mole fraction~~concentration~~s to see how the different models affect tracer transport.

16

3.4 Seasonal analysis

3.4.1 Annual gradient

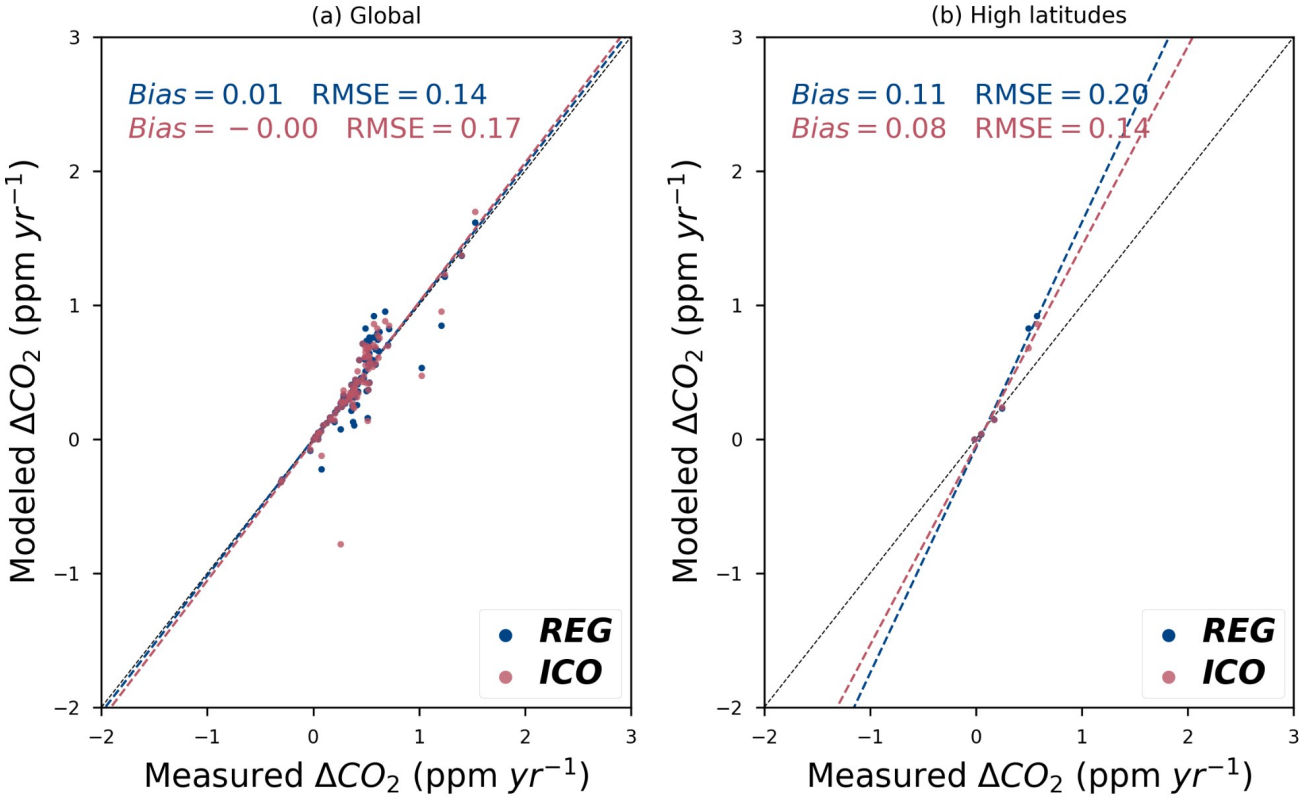

17

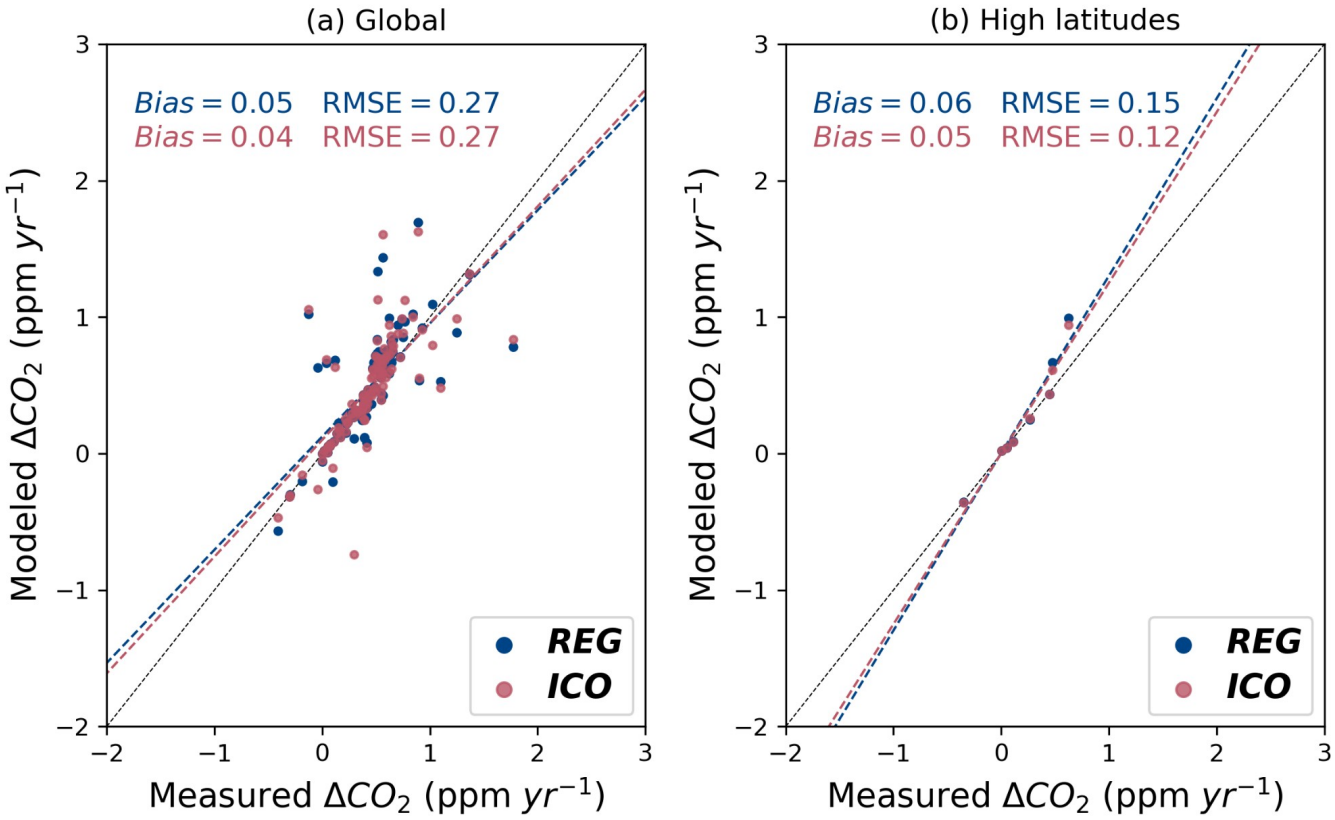

Figure 64: Annual gradients of CO_2 mole fraction~~mixing ratio~~ compared to SPO averaged over the 1980-2020 period for every station (a) or only stations at high latitudes (> 70°N/S) (b). Blue circles are the model outputs for the REG configuration, and red circles for the ICO configuration. The dotted lines correspond to the linear fitted lines of the corresponding colored configurations, and the black dotted lines correspond to the 1:1 relation.

Figure 64 shows the annual gradients of surface stations compared to SPO averaged over the 1980-2020 period, and for the two model configurations the differences between the modeled and observed values of this gradient. We find an average yearly growth rate of CO_2 mole fraction~~mixing ratio~~ at SPO of 1.79 ppm per year from observations, and of 1.74 ppm per year for both the REG and ICO configurations. This difference of 0.05 ppm between our models and observations shows that the background growth rate of CO_2 mole fraction~~concentration~~ is well modeled and within the small uncertainty range of the observations.

When looking at all surface stations (a), the ICO configuration exhibits a ~~slightly lower overall~~ bias that is not significantly different from the REG configuration, ~~but~~and an almost identical spread as seen by the root mean square error (RMSE). Both configurations show a ~~positive~~ bias of less than 0.1 ppm per year compared to observations. The two model configurations therefore successfully model the annual gradients between surface stations over the globe.

18

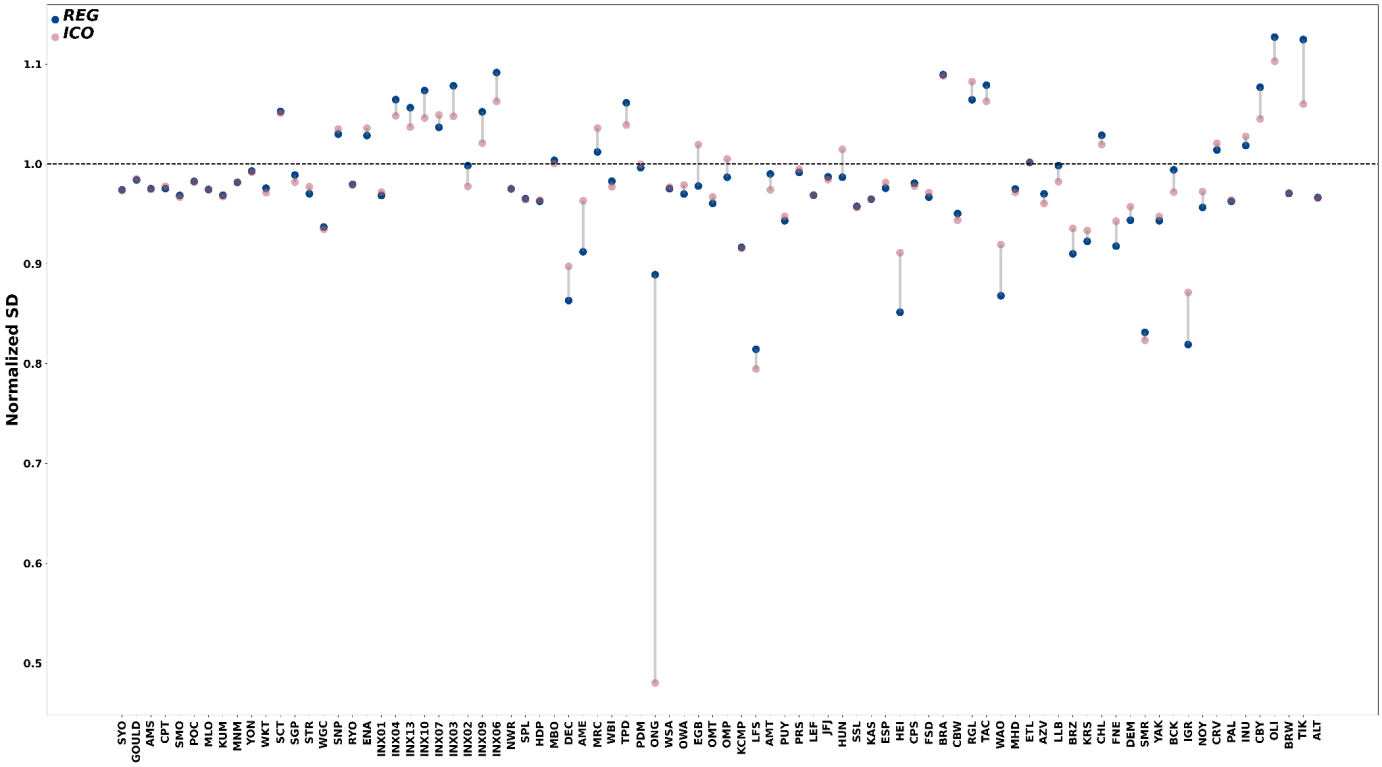
REG
ICO
Normalized SD
1.1
1.0
0.9
0.8
0.7
0.6
0.5
SYO GOULD AMS CPT SMO POC MLO KUM MNM YON WKT SCT SGP STR WGC SNP RYO ENA INX01 INX04 INX13 INX10 INX07 INX03 INX02 INX09 INX06 NWR SPL HDP MBO DEC AME MRC WBI TPD PDM ONG WSA OWA EGB OMT OMP KCMP LFS AMT PUY PRS LEF JFJ HUN SSL KAS ESP HEI CPS FSD BRA CBW RGL TAC WAO MHD ETL AZV LLB BRZ KRS CHL FNE DEM SMR YAK BCK IGR NOY CRV PAL INU CBY OLI BRW TIK ALT

442

19

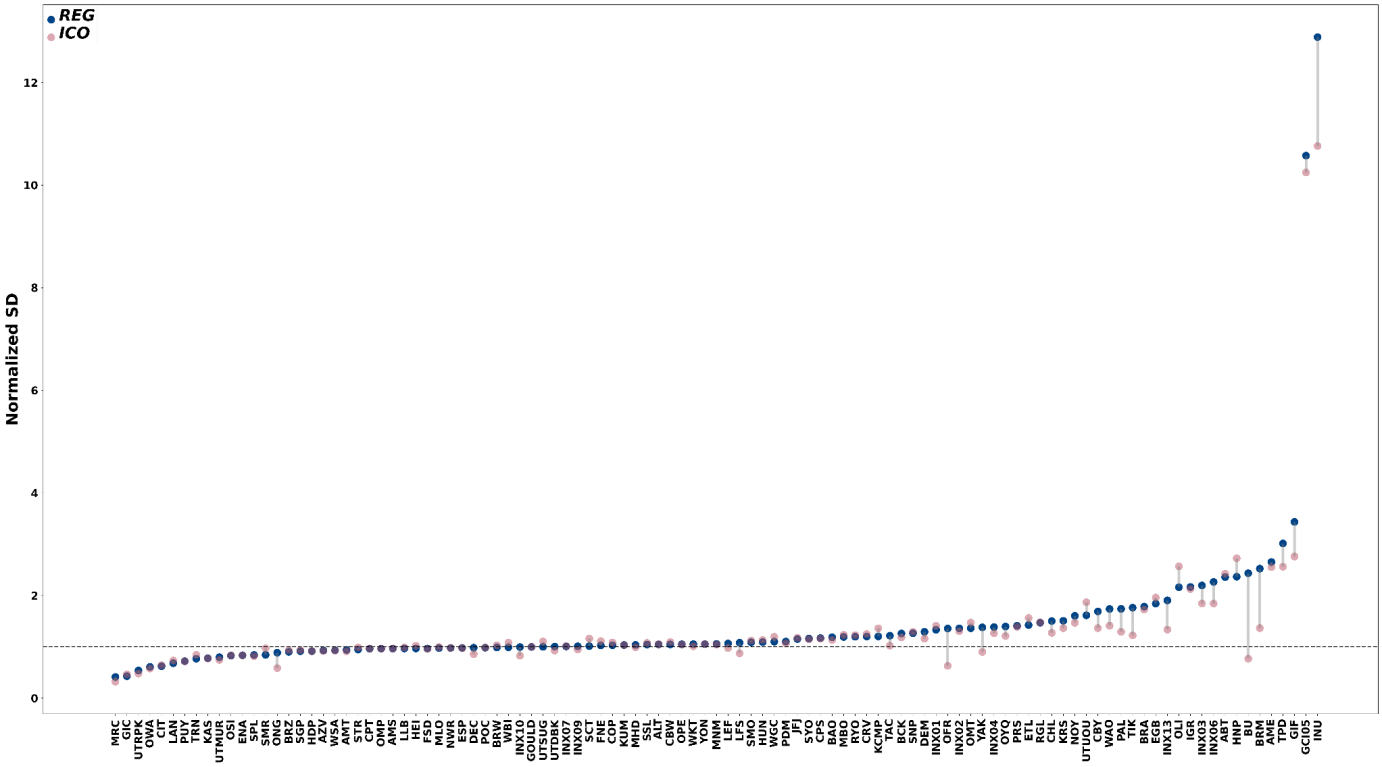

Figure 75: Normalized standard deviation of the annual gradient for both configurations for each station. Blue circles are the model outputs for the REG configuration, and red circles for the ICO configuration. The dotted line corresponds to the ideal normalized standard deviation of 1. The stations are ordered on the abscissa by increasing latitude from -90° to +90°.

The average normalized standard deviation of the interannual variation in the annual gradient for both configurations is 1.01,~~the REG configuration is 1.43 and 1.37 for the ICO configuration. ICO therefore better captures the temporal variations of this gradient, but~~ therefore both configurations show a good agreement in magnitude of these variations for the majority of stations (Fig. 7).

Since the biggest change regarding the grid and resolution takes place at the poles, we also checked the statistics and linear fit of these gradients restricted to stations at high latitudes (higher than 70°N and lower than 70°S). ICO performs just as well as REG for these stations in terms of both general bias and spread (Fig. 64 (b)). Even though the spatial~~effective~~ resolution is much coarser for the ICO configuration at these latitudes, it has not significantly affected the simulation of long term trends of CO_2 mole fraction~~concentration~~s. We can also verify this by looking at the bias in the annual gradient of CO_2 mole fraction per station (Fig. 8) according to latitude. We see that there is no difference in between the two configurations related to latitude. This shows that forced resolution clustering at the poles of the regular latitude-longitude grid is not necessary for properly resolving tracer transport.

20

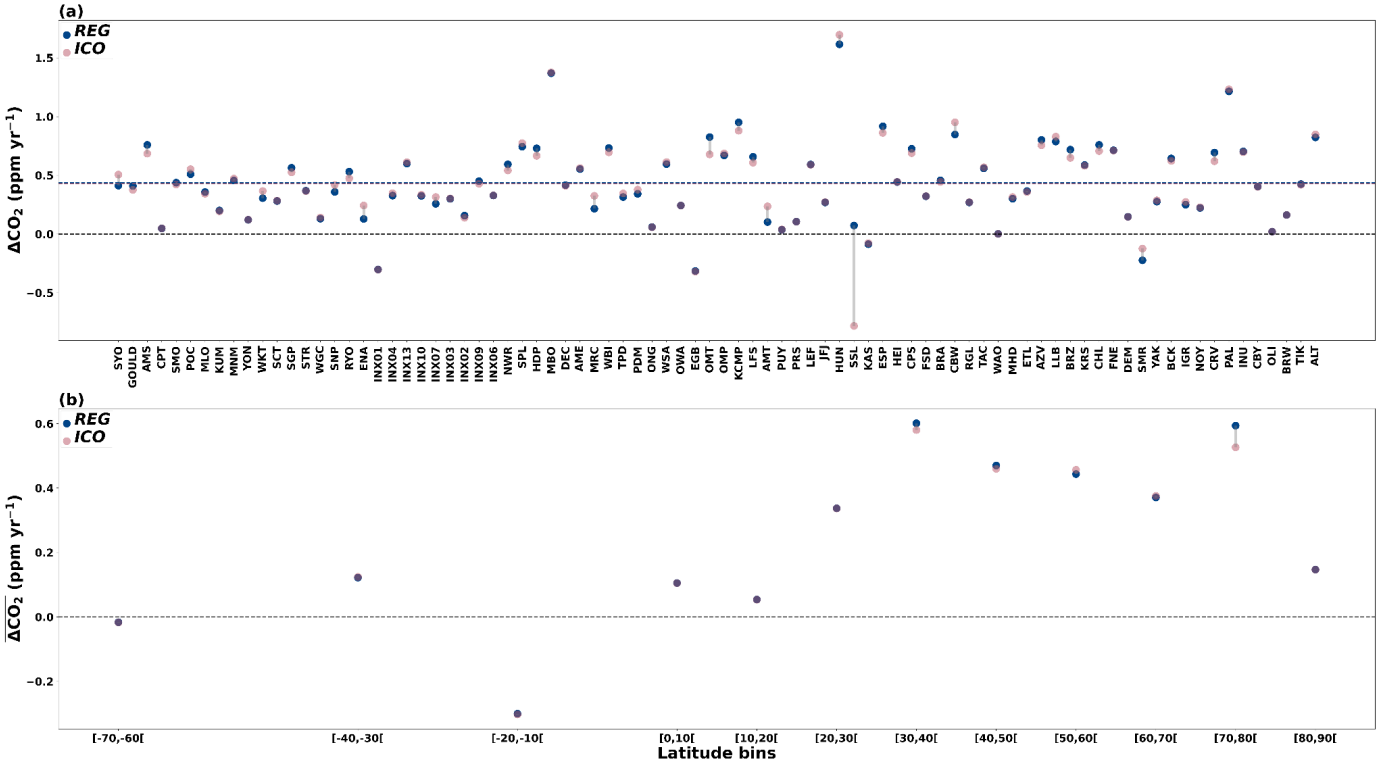

Figure 8: Bias per station (a) and average bias per 10° latitude band (b) of the annual gradients of CO2 mole fraction compared to SPO averaged over the period 1980-2020, with blue circles for REG and red circles for ICO, the gray line is the difference between the two. The stations in (a) are ordered on the abscissa by increasing latitude from -90° to +90°.

21

3.4.2 Seasonal cycle

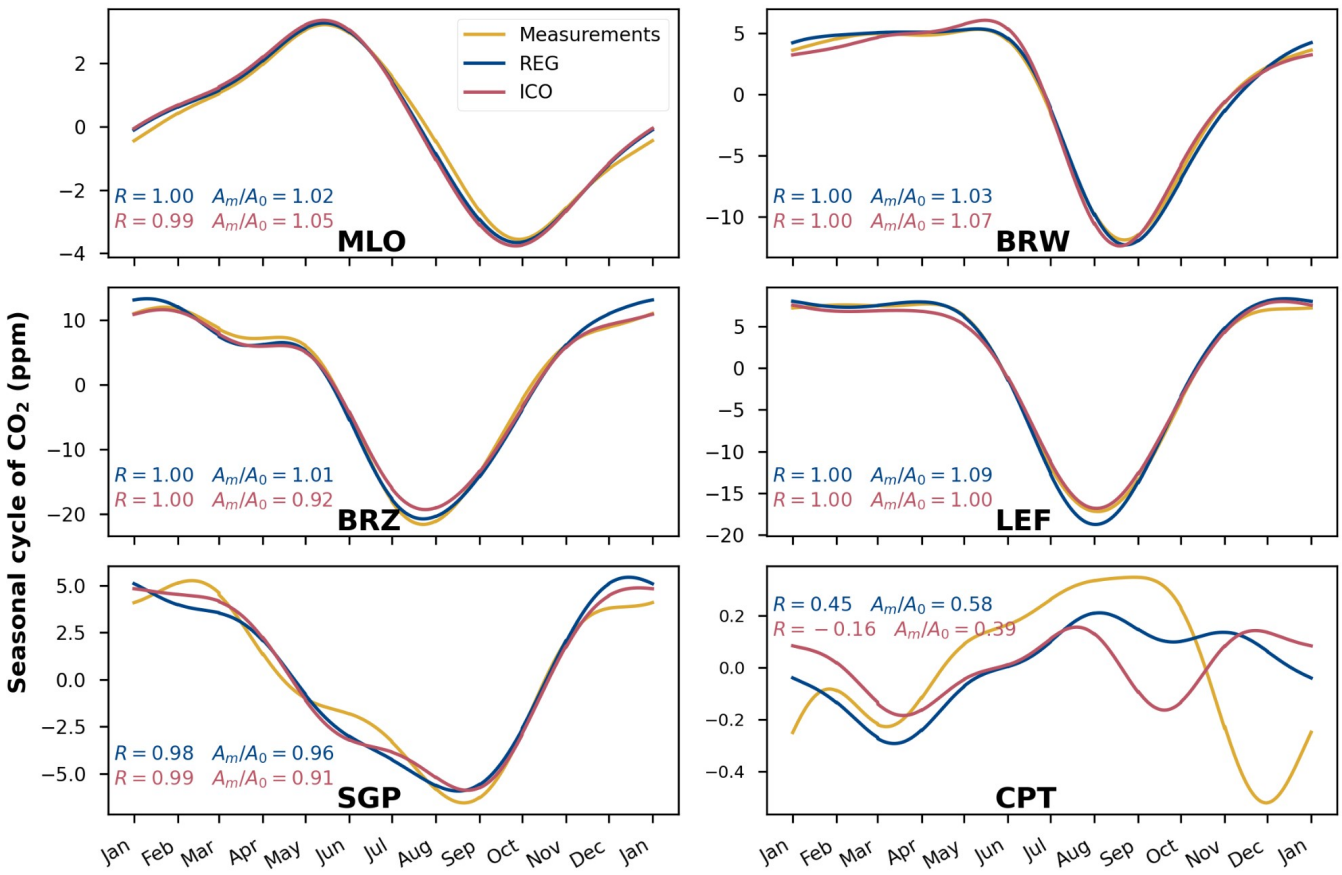

22

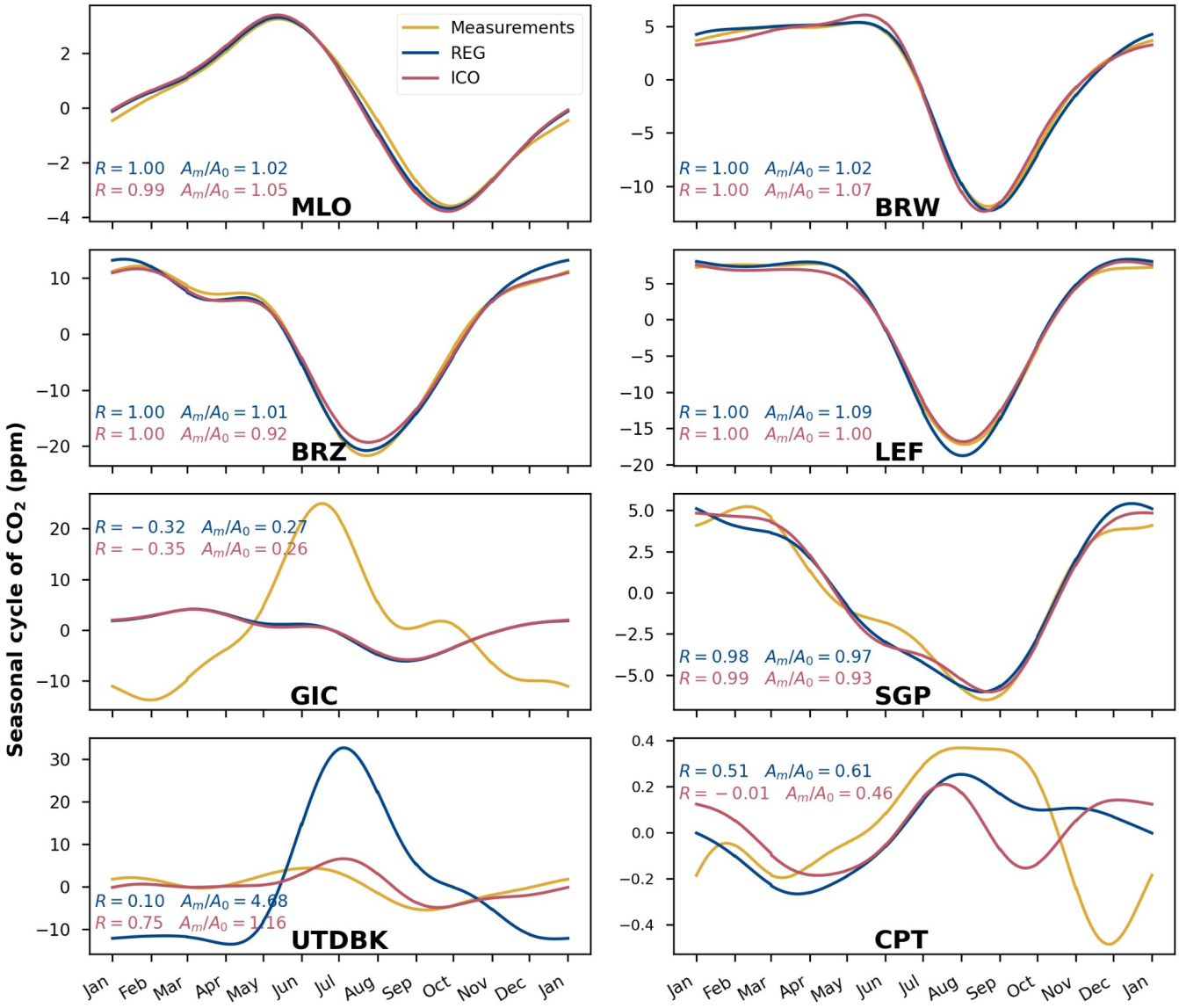

Figure 96: Seasonal cycle of the CO2 mole fraction~~mixing ratio~~ averaged over the period 1980-2020, in ppm, at a selection of surface stations for measurements, REG configuration and ICO configuration in yellow, blue and red respectively. The correlation coefficient and the peak-to-peak amplitude between the two model's output and measurements are displayed for each station. The selected stations were chosen to exemplify diverse behaviors: where both configurations successfully capture the seasonal cycle, neither configuration does so, or only one out of the two model configurations achieves it.

The seasonal cycles at most surface stations are well captured by both configurations, with regards to both phase and amplitude, as illustrated in Fig. 96. Some stations exhibiting more complex and higher frequency patterns of CO_2 mole fraction~~concentration~~s variation throughout seasons have a lower correlation coefficient. This pattern is observed for both configurations. However, almost all stations that are adequately modeled by the REG configuration with regards to seasonal cycles (correlation coefficient higher than 0.8) are equally well represented in the ICO configuration, as shown in Fig. ~~7~~10 (a). Out of the 85~~107~~ stations analyzed, only 3~~12~~ stations did not exceed a correlation of 0.8 with either~~the~~ REG configuration.~~, and~~

23

~~11 with the ICO configuration. Additionally, no station exhibited satisfactory performance with REG but not with ICO, while the opposite was true for one station.~~ Only one station, CPT, performs significantly worse for the ICO configuration than for the REG configuration. The amplitude of the seasonal cycle is also well captured for almost all stations, as shown in Fig. 10~~7~~ (b).

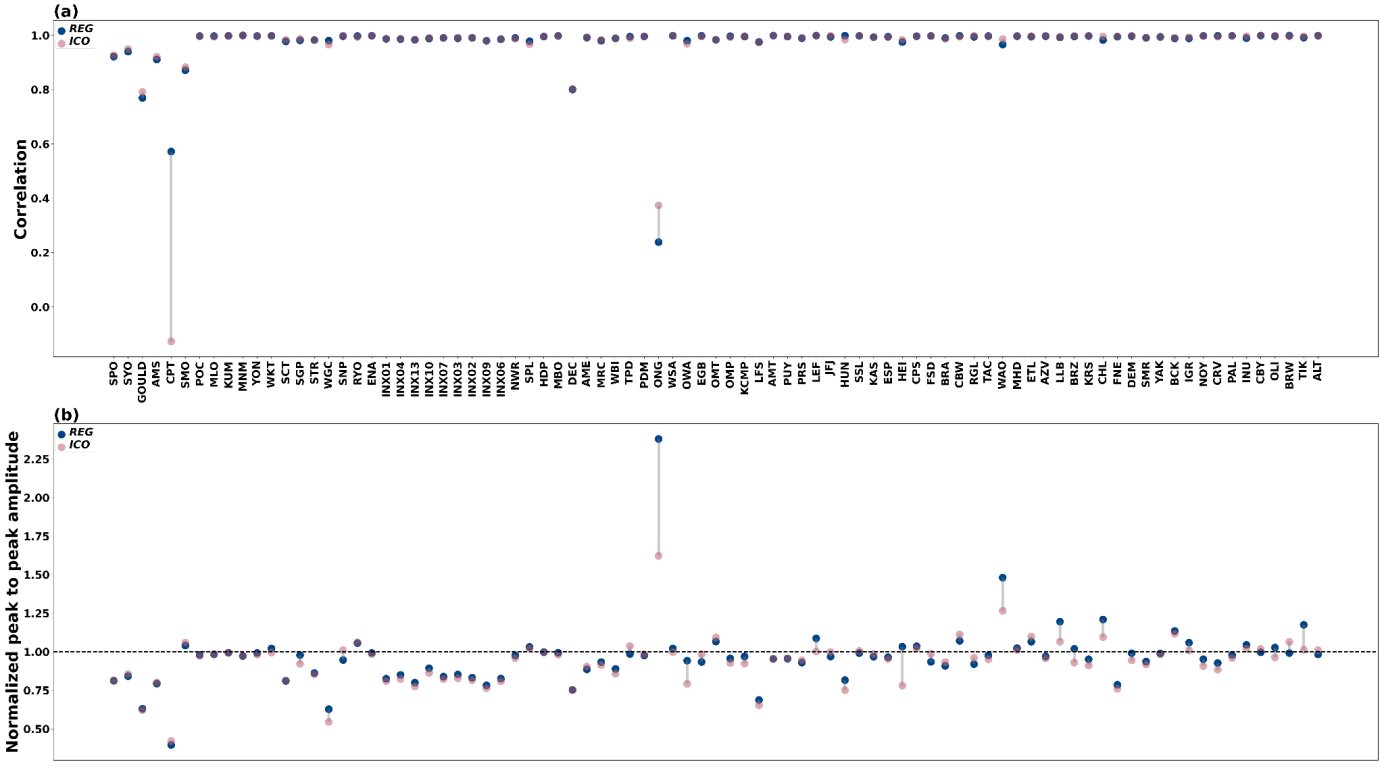

24

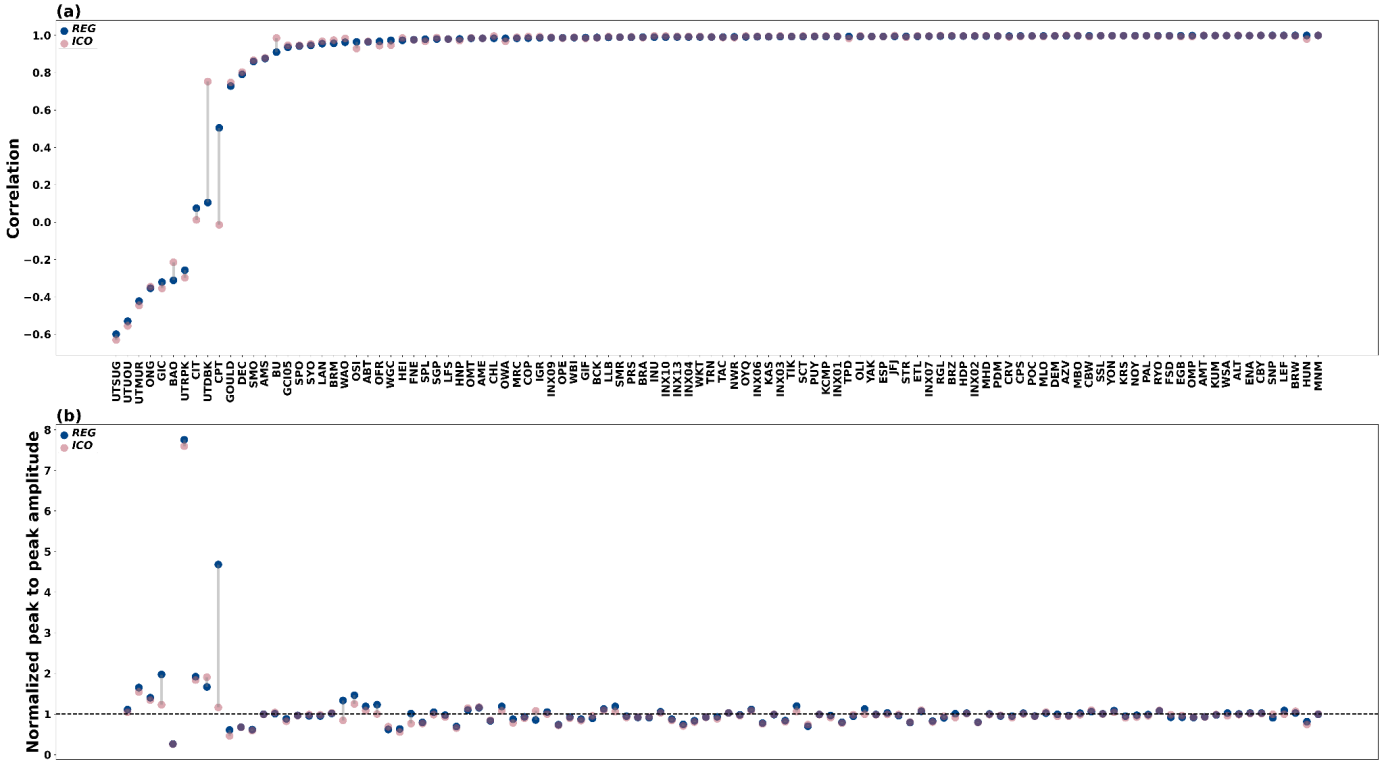

Figure 107: Pearson correlation coefficient (a) and normalized standard deviation (b) of the seasonal cycle for all surface stations studied averaged over the period 1980-2020, with blue circles for REG and red circles for ICO, the gray line is the difference between the two. The stations are ordered on the abscissa by increasing latitude from -90° to +90°~~by increasing correlation coefficient for REG~~.

3.4.2 Synoptic variability

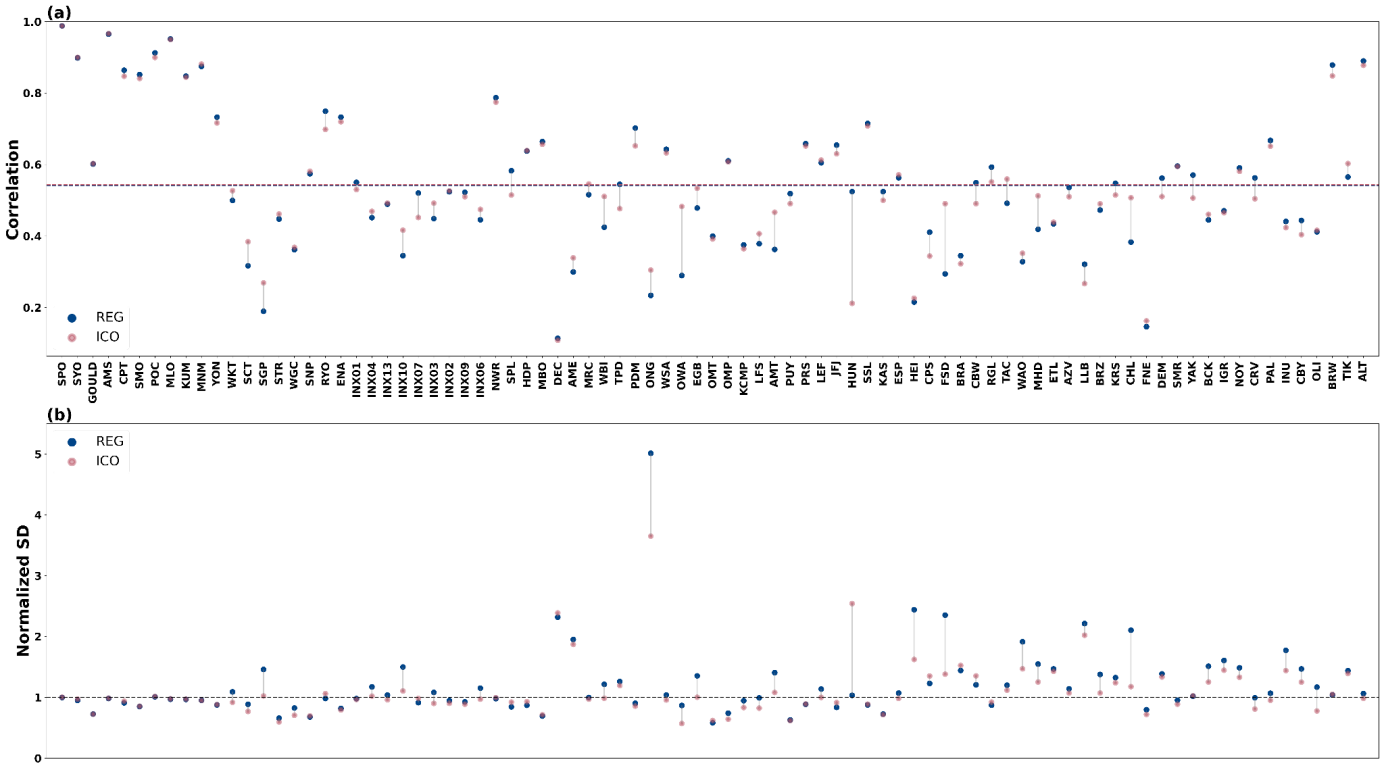

25

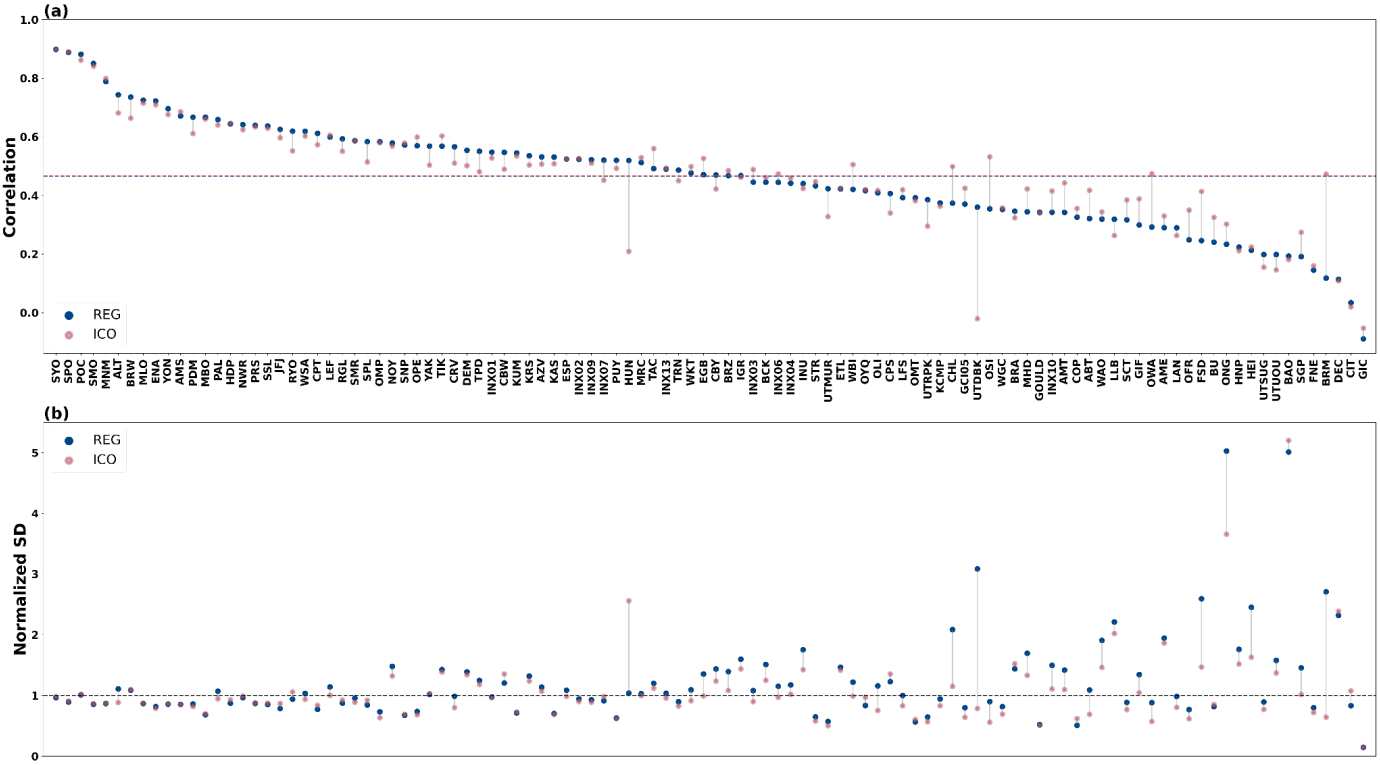

Figure ~~8~~11: Pearson correlation (a) and normalized standard deviation (b) of the daily average residue between our modeled and measured CO_2 mole fraction~~concentration~~s at the surface stations described in section 2.5 for the period 1980-2020. The model output from the REG and ICO configurations are in blue and red respectively. The stations are ordered on the abscissa by increasing latitude from -90° to +90°.

To study the synoptic variability modeled by our two model configurations, we look at the correlation and the normalized standard deviation (NSD) of the daily averaged residue of our seasonal analysis for each surface station (Fig. 11). This gives us information on the accuracy of our simulation for higher frequency than the seasonal cycles. Both configurations have correlation coefficients over 0.6357 for 25% of all stations and a mean value of 0.5447 for REG and ICO. The ICO configuration has a lower mean NSD of 1.096 compared to the one of REG of 1.20. And stations that offer a good correlation also tend to exhibit a better spread of the synoptic variability characterized by the NSD. These results are in line with what can be expected of a simulation at these resolutions as shown in Agustí-Panareda et al. (2019).

26

3.5 Vertical profiles of CO_2 mole fraction~~concentration~~s

3.5.1 Troposphere

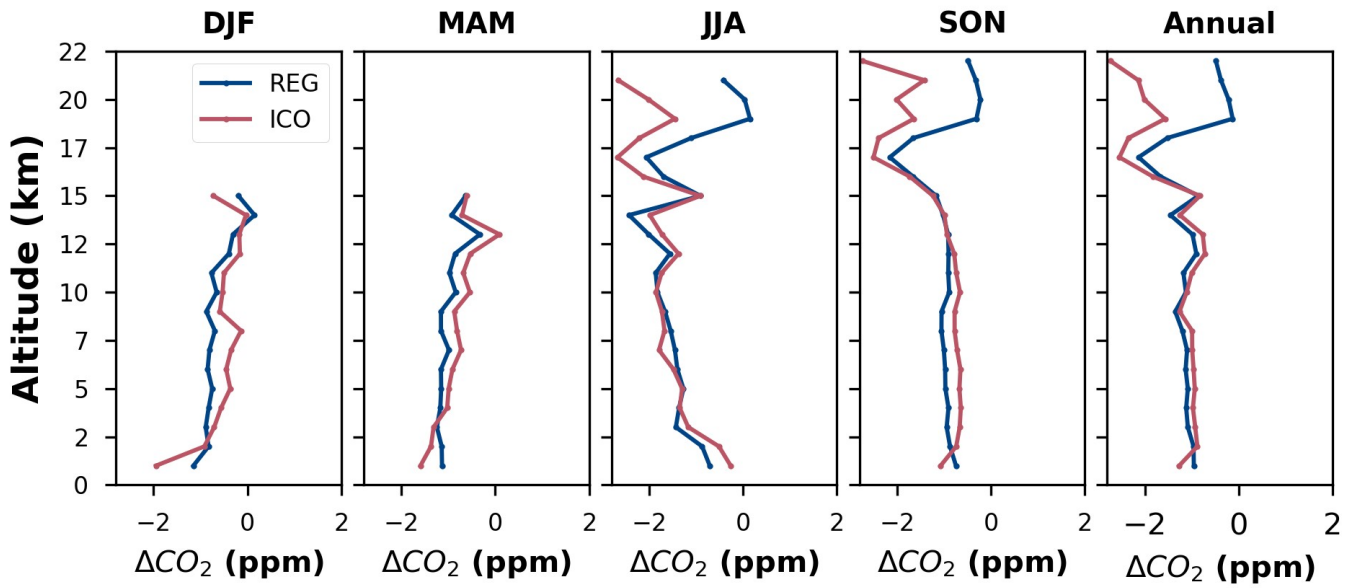

Figure 129: Seasonal and annual means of the difference in CO_2 vertical profile between the two model configurations of the model and aircraft measurements. The data has been binned into 1 km altitude bins for each season of the 1980-2020 period, then averaged per hour, and finally averaged across all aircraft sites and campaigns. The blue line represents the difference between REG and the measurements, while the red line represents the difference between ICO and the measurements.

In the troposphere, we studied CO_2 vertical profiles using various aircraft measurements described in section 2.4.2. Figure 129 shows the differences between the simulated and observed values for our two model configurations, REG and ICO. Only a small number of aircraft campaigns reach high altitudes above 15 km and not all seasons are covered. Both configurations show very similar vertical profiles up to 15 km altitude, before diverging above. Both configurations show a general negative bias compared to measurements. The vertical profiles~~variations in vertical gradients~~ are almost identical for all altitudes, but the extent of the differences between model's output and measurements differ at high altitudes. REG has much greater variations in CO_2 mole fraction~~concentration~~s while ICO has an increased negative bias at high altitudes. This is similar to the results in the next section 3.5.2.

3.5.2 Low stratosphere

We utilized data from AirCore flights to compare the CO_2 mole fractions~~mixing ratios~~ of our model with observed data and obtain vertical profiles extending to the low stratosphere, in order to investigate the potential effects of the change in dynamics on vertical mixing within a column. However, since these measurements were only conducted in latitudes higher than 30°N and lower than 30°S, information about vertical tracer transport in the tropics was not obtained. As shown in Fig. 130, both model configurations exhibit an excess of CO_2 mole fraction~~concentration~~s around the 12.5 km range. Above that altitude, the vertical profiles differ in amplitude between the configurations but both show a similar decrease in CO_2 mole fraction. ~~However, the REG configuration has an additional peak in CO_2~~ mole fraction~~concentrations at 20 km, followed by a gradient change and a subsequent decrease in~~ mole fraction~~concentration at higher altitudes. In contrast, the ICO configuration does not display the same peak at 20 km, but a similar gradient change is observed above this altitude. This finding suggests that tracer vertical transport is inadequate between the low and high stratosphere at these latitudes, and CO_2 accumulates at lower levels than~~

27

expected for the REG configuration. While the ICO configuration employs the same van Leer vertical transport scheme, differences in the vertical temperature profiles (see Fig. 42 and Fig. 53) discussed in section 3.4 could explain the disparity in the amplitude of the vertical profile at the stratosphere. The attribution of this systematic error to a particular process is complicated by the high potential collection altitude determination error of AirCore measurements, which can be on the order of a kilometer in the stratosphere as discussed briefly in section 2.3 (Wagenhäuser et al., 2021). The previously discussed conclusions however are independently verified by the aircraft measurements that do not suffer from the Aircore altitude determination error and show similar differences in CO_2 mole fractionconcentrations at 20 km (Fig. 912).

28

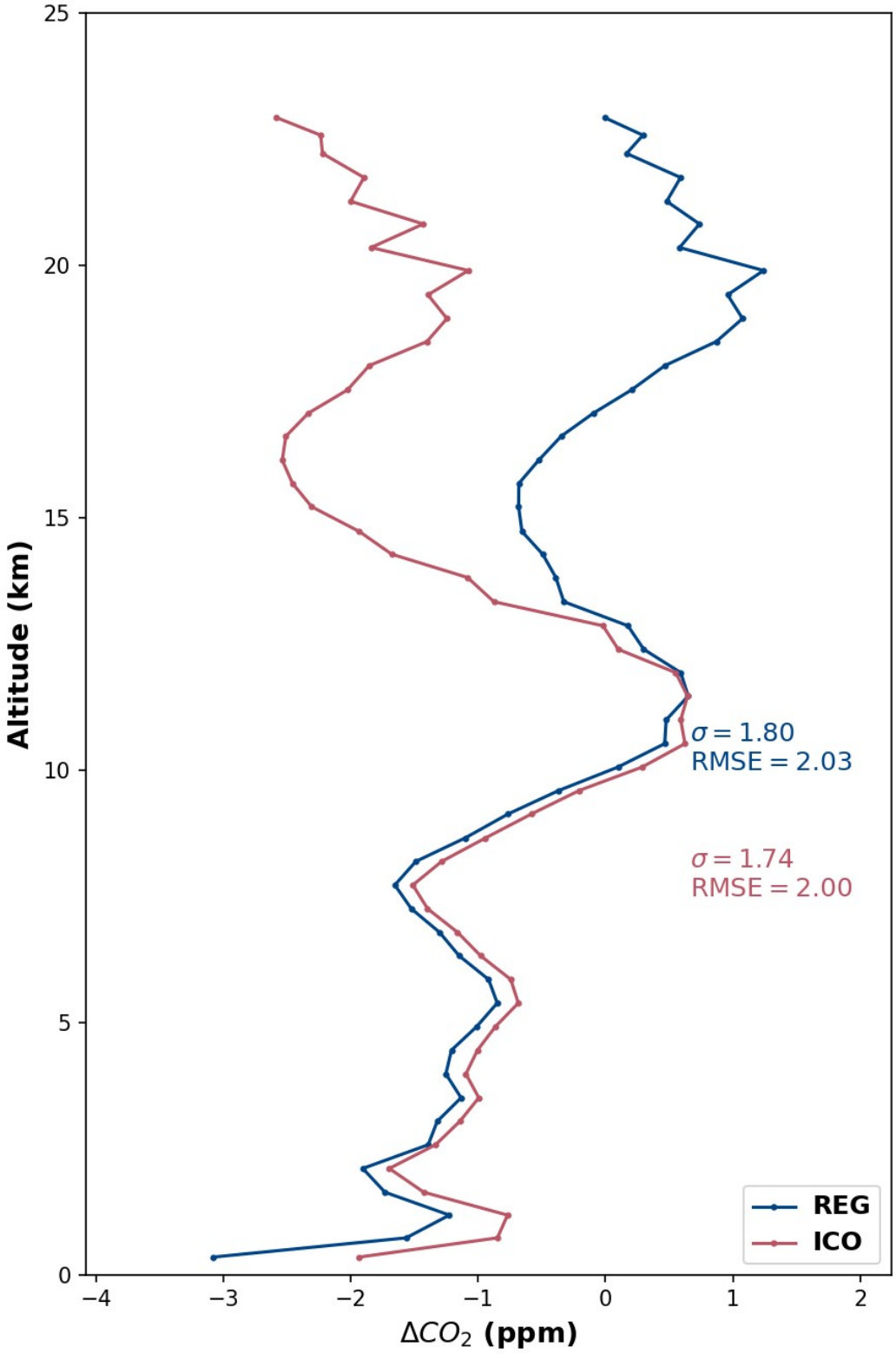
25
20
15
10
5
0
−4
−3
−2
−1
0
1
2
Altitude (km)
ΔCO_2 (ppm)
$\sigma = 1.80$
RMSE = 2.03
$\sigma = 1.74$
RMSE = 2.00
REG
ICO

533

29

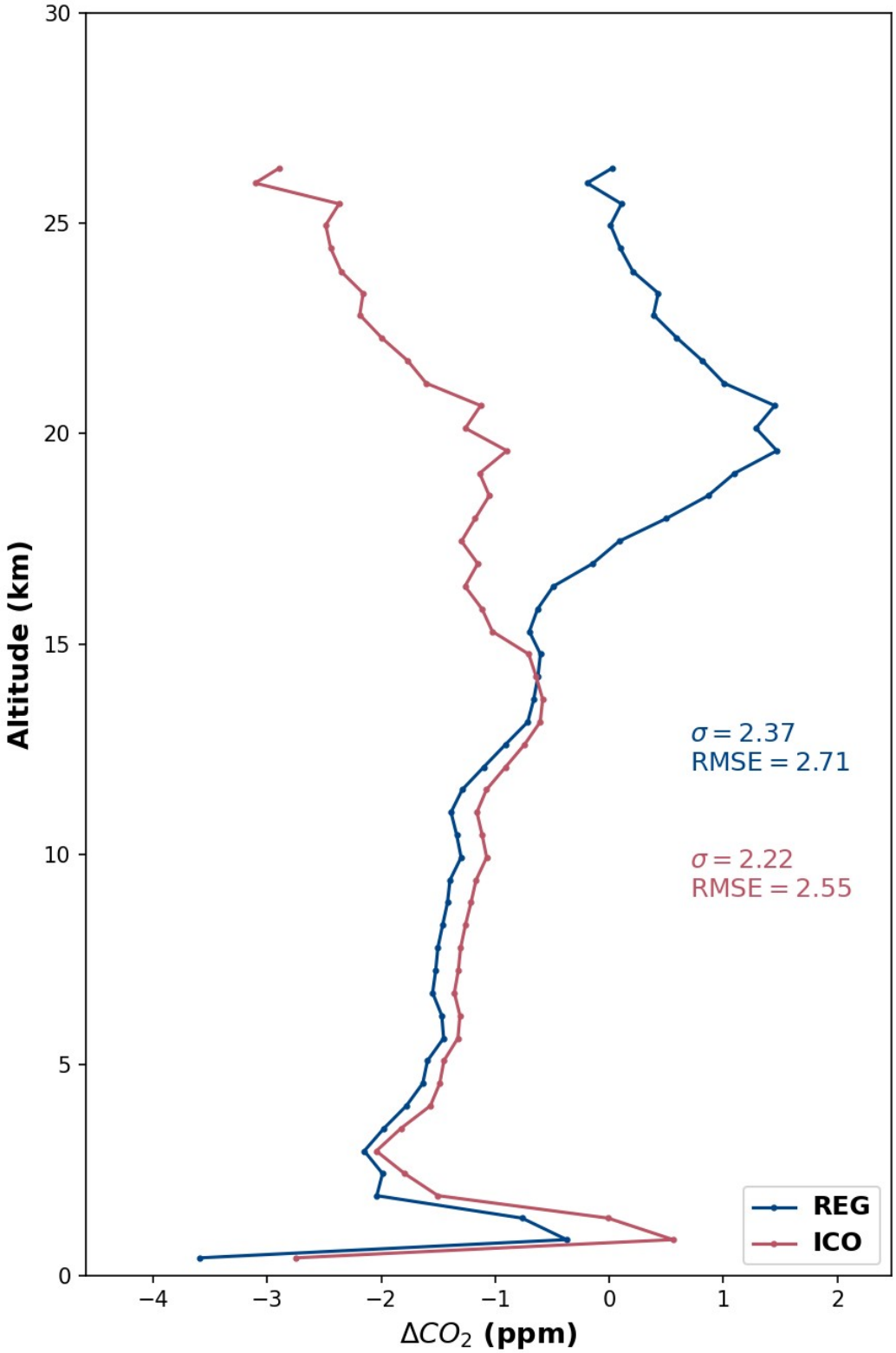

534

535 **Figure 1~~0~~3: Difference in CO_2 mole fraction~~mixing ratio~~ vertical profile between the two model configurations of the model and**
536 **AirCore measurements. The blue line represents the difference between the REG model output and measurements, while the red line**
537 **indicates the difference between the ICO model output and measurements. The fitted lines were generated by averaging the data over**
538 **50 altitude bins.**

30

4 Conclusion

As demonstrated in the previous section's results, the configuration ICO based on the new dynamical core DYNAMICO~~Dynamico~~, using an unstructured grid is just as effective as the reference configuration that used a structured latitude-longitude grid for modeling atmospheric CO_2 transport when the dynamics was nudged to horizontal winds of an ERA5 reanalysis. Both configurations accurately capture the seasonal variations in CO_2 mole fraction~~concentration~~s at most surface stations, and while the ICO configuration did not better capture more complex seasonal patterns, it did not worsen it either. ~~A low percentage of station's seasonal cycles are properly captured by only one of the two model configurations.~~ The annual gradient is almost identical between both configurations, and they both perform well regardless of latitude ~~between stations exhibit slightly higher overall bias with ICO than with REG, but ICO has a smaller dispersion compared to observations~~. Regarding synoptic variability both configurations also perform almost identically.~~, the ICO configuration generally exhibits a lower correlation but a smaller standard deviation in comparison to observations.~~ Nevertheless, both configurations provide an inadequate modeling of synoptic variability, as the local high-frequency emissions are poorly constrained and the horizontal resolution is still too coarse.

Additionally, both configurations offer comparable vertical CO_2 mole fraction~~concentration~~ profiles and exhibit the same bias in the lower stratosphere relative to observational data. In contrast, gravity waves in the new ICO configuration may need some tuning in order to improve the quality of temperature at the tropopause and in the stratosphere (Lott et al., 2005). Their impact on atmospheric transport of CO_2 at lower altitudes has not been specifically evaluated but seems~~is expected~~ to be minimal given the small differences shown between the two model configurations. Tuning ~~of the climatology of~~ the LMDZ - DYNAMICO~~Dynamico~~ coupling in general is still an ongoing process.

The new ICO configuration offers new opportunities in terms of development. Its use of fewer cells per level for a comparable resolution at the equator results in faster computation times of around 20% in our main simulation~~tests~~ and easier-to-store outputs thanks to their smaller size on disk. Unlike regular latitude-longitude grids, ICO does not require a polar filter, whereas these filters generally parallelize badly, on both CPU and GPU. ICO~~It~~ provides~~gives~~ a more homogeneous grid compared to the grid clustering~~higher resolution~~ at the poles of a regular latitude-longitude grid ~~which is not always needed for modelisation at a global scale~~. The ICO configuration also allows for much better scaling of computing resources when used at higher resolution, increasing even further the computational speed of the simulations relative to the structured latitude-longitude grid.

While running, REG and ICO can archive specific meteorological variables like air mass fluxes which can then be read by an offline version of the model dedicated to tracer transport. This economical transport model forms the basis of the inversion system of Chevallier et al. (2005) to generate the CO_2 and N_2O inversion products of the Copernicus Atmosphere Monitoring Service of the European Commission (CAMS service, (https://atmosphere.copernicus.eu/ghg-services). Our next task is the implementation of DYNAMICO~~Dynamico~~ in this offline model in order to prepare future resolution increases, while limiting~~damping~~ the induced increase in computational cost~~of the code time-to-solution~~.

Code and data availability

The source code for the REG and ICO configurations is freely available online via the following address: https://forge.ipsl.jussieu.fr/igcmg/browser/CONFIG/publications/ICOLMDZORINCA_CO2_Transport_GMD_2023

under the CeCILL v2 Free Software License (http://www.cecill.info/index.en.html, last access: 11 September 2023, CECILL,

2020). The exact version of the model used to produce the results used in this paper is archived on Zenodo, as are input data and scripts to run the model and produce the plots for all the simulations presented in this paper (Lloret et al., 2023).

Author contributions

ZL designed, ran and analyzed the simulations and prepared the paper under direction and advice of FC. AC contributed to the development and preparation of the simulations. MR was also involved in the development of the simulations. YM supported the development of the model. All authors contributed to the text.

Disclaimer

The authors declare that they have no conflict of interest.

Acknowledgements

This work was granted access to the HPC resources of TGCC under the allocation A0130102201 made by GENCI. It was funded by the Copernicus Atmosphere Monitoring Service, implemented by ECMWF on behalf of the European Commission (Grant: CAMS2 55). We thank Olivier Boucher for fruitful discussions on vertical temperature profiles and the LMDZ model, and Sakina Takache for discussions on DYNAMICO~~Dynamico~~. We also thank Julien Derouillat for his help in the implementation of XIOS for our application. We also gratefully acknowledge the many people who contributed atmospheric observations (aircraft, AirCore and surface air sample measurements). Measurements at Jungfraujoch were supported by ICOS Switzerland, which is funded by the Swiss National Science Foundation, in-house contributions and the State Secretariat for Education, Research and Innovation. We thank Kathryn McKain for her comments and suggestions on the best way to describe aircraft and AirCore data. We also thank Bianca Baier for her help with the AirCore data.

References

Agustí-Panareda, A., Diamantakis, M., Massart, S., Chevallier, F., Muñoz-Sabater, J., Barré, J., Curcoll, R., Engelen, R., Langerock, B., Law, R. M., Loh, Z., Morguí, J. A., Parrington, M., Peuch, V.-H., Ramonet, M., Roehl, C., Vermeulen, A. T., Warneke, T., and Wunch, D.: Modelling CO_2 weather – why horizontal resolution matters, Atmospheric Chemistry and Physics, 19, 7347–7376, https://doi.org/10.5194/acp-19-7347-2019, 2019.

Agustí-Panareda, A., McNorton, J., Balsamo, G., Baier, B. C., Bousserez, N., Boussetta, S., Brunner, D., Chevallier, F., Choulga, M., Diamantakis, M., Engelen, R., Flemming, J., Granier, C., Guevara, M., Denier van der Gon, H., Elguindi, N., Haussaire, J.-M., Jung, M., Janssens-Maenhout, G., Kivi, R., Massart, S., Papale, D., Parrington, M., Razinger, M., Sweeney, C., Vermeulen, A., and Walther, S.: Global nature run data with realistic high-resolution carbon weather for the year of the Paris Agreement, Sci Data, 9, 160, https://doi.org/10.1038/s41597-022-01228-2, 2022.

Baier, B., Sweeney, C., Newberger, T., Higgs, J., Wolter, S., & NOAA Global Monitoring Laboratory. NOAA AirCore atmospheric sampling system profiles (Version 20230831) [Data set]. NOAA GML. https://doi.org/10.15138/6AV0-MY81, 2021.

Basu, S., Baker, D. F., Chevallier, F., Patra, P. K., Liu, J., and Miller, J. B.: The impact of transport model differences on CO_2 surface flux estimates from OCO-2 retrievals of column average CO_2, Atmospheric Chemistry and Physics, 18, 7189–7215, https://doi.org/10.5194/acp-18-7189-2018, 2018.

Cadule, P., Friedlingstein, P., Bopp, L., Sitch, S., Jones, C. D., Ciais, P., Piao, S. L., and Peylin, P.: Benchmarking coupled climate-carbon models against long-term atmospheric CO2 measurements, Global Biogeochemical Cycles, 24, https://doi.org/10.1029/2009GB003556, 2010.

CeCILL: CeCILL and Free Software, http://www.cecill.info/index.en.html (last access: 3 July 2023), 2020.

32

Chau, T. T. T., Gehlen, M., and Chevallier, F.: A seamless ensemble-based reconstruction of surface ocean pCO2 and air–sea CO2 fluxes over the global coastal and open oceans, Biogeosciences, 19, 1087–1109, https://doi.org/10.5194/bg-19-1087-2022, 2022.

~~Chevallier, F., M. Fisher, P. Peylin, S. Serrar, P. Bousquet, F.-M. Bréon, A. Chédin, and P. Ciais, 2005: Inferring CO2 sources and sinks from satellite observations: method and application to TOVS data. J. Geophys. Res., 110, D24309, doi:10.1029/2005JD006390.~~

Chevallier, F., Fisher, M., Peylin, P., Serrar, S., Bousquet, P., Bréon, F.-M., Chédin, A., and Ciais, P.: Inferring CO2 sources and sinks from satellite observations: Method and application to TOVS data, Journal of Geophysical Research: Atmospheres, 110, https://doi.org/10.1029/2005JD006390, 2005.

Chevallier, F., Ciais, P., Conway, T. J., Aalto, T., Anderson, B. E., Bousquet, P., Brunke, E. G., Ciattaglia, L., Esaki, Y., Fröhlich, M., Gomez, A., Gomez-Pelaez, A. J., Haszpra, L., Krummel, P. B., Langenfelds, R. L., Leuenberger, M., Machida, T., Maignan, F., Matsueda, H., Morguí, J. A., Mukai, H., Nakazawa, T., Peylin, P., Ramonet, M., Rivier, L., Sawa, Y., Schmidt, M., Steele, L. P., Vay, S. A., Vermeulen, A. T., Wofsy, S., and Worthy, D.: CO2 surface fluxes at grid point scale estimated from a global 21 year reanalysis of atmospheric measurements, Journal of Geophysical Research: Atmospheres, 115, https://doi.org/10.1029/2010JD013887, 2010.

Chevallier, F., Lloret, Z., Cozic, A., Takache, S., and Remaud, M.: Toward High-Resolution Global Atmospheric Inverse Modeling Using Graphics Accelerators, Geophysical Research Letters, 50, e2022GL102135, https://doi.org/10.1029/2022GL102135, 2023.

Ciais, P., Dolman, A. J., Bombelli, A., Duren, R., Peregon, A., Rayner, P. J., Miller, C., Gobron, N., Kinderman, G., Marland, G., Gruber, N., Chevallier, F., Andres, R. J., Balsamo, G., Bopp, L., Bréon, F.-M., Broquet, G., Dargaville, R., Battin, T. J., Borges, A., Bovensmann, H., Buchwitz, M., Butler, J., Canadell, J. G., Cook, R. B., DeFries, R., Engelen, R., Gurney, K. R., Heinze, C., Heimann, M., Held, A., Henry, M., Law, B., Luyssaert, S., Miller, J., Moriyama, T., Moulin, C., Myneni, R. B., Nussli, C., Obersteiner, M., Ojima, D., Pan, Y., Paris, J.-D., Piao, S. L., Poulter, B., Plummer, S., Quegan, S., Raymond, P., Reichstein, M., Rivier, L., Sabine, C., Schimel, D., Tarasova, O., Valentini, R., Wang, R., van der Werf, G., Wickland, D., Williams, M., and Zehner, C.: Current systematic carbon-cycle observations and the need for implementing a policy-relevant carbon observing system, Biogeosciences, 11, 3547–3602, https://doi.org/10.5194/bg-11-3547-2014, 2014.

Crotwell, A., Lee, H., Steinbacher, M., Eds.: “20th WMO/IAEA Meeting on Carbon Dioxide, Other Greenhouse Gases and Related Measurement Techniques (GGMT-2019),” GAW REPORT No. 255 (World Meteorological Organization, 2020); https://library.wmo.int/doc_num.php?explnum_id=10353, 2020.

Dubey, S., Dubos, T., Hourdin, F., and Upadhyaya, H. C.: On the inter-comparison of two tracer transport schemes on icosahedral grids, Applied Mathematical Modelling, 39, 4828–4847, https://doi.org/10.1016/j.apm.2015.04.015, 2015.

Dubos, T. and Tort, M.: Equations of Atmospheric Motion in Non-Eulerian Vertical Coordinates: Vector-Invariant Form and Quasi-Hamiltonian Formulation, Monthly Weather Review, 142, 3860–3880, https://doi.org/10.1175/MWR-D-14-00069.1, 2014.

Dubos, T., Dubey, S., Tort, M., Mittal, R., Meurdesoif, Y., and Hourdin, F.: DYNAMICO-1.0, an icosahedral hydrostatic dynamical core designed for consistency and versatility, Geosci. Model Dev., 8, 3131–3150, https://doi.org/10.5194/gmd-8-3131-2015, 2015.

Ducoudré, N. I., Laval, K., and Perrier, A.: SECHIBA, a New Set of Parameterizations of the Hydrologic Exchanges at the Land-Atmosphere Interface within the LMD Atmospheric General Circulation Model, J. Climate, 6, 248–273, https://doi.org/10.1175/1520-0442(1993)006<0248:SANSOP>2.0.CO;2, 1993.

Emanuel, K. A.: A Scheme for Representing Cumulus Convection in Large-Scale Models, Journal of the Atmospheric Sciences, 48, 2313–2329, https://doi.org/10.1175/1520-0469(1991)048<2313:ASFRCC>2.0.CO;2, 1991.

Evangeliou, N., Balkanski, Y., Cozic, A., and Møller, A. P.: Simulations of the transport and deposition of ¹³⁷Cs over Europe after the Chernobyl Nuclear Power Plant accident: influence of varying emission-altitude and model horizontal and vertical resolution, Atmos. Chem. Phys., 13, 7183–7198, https://doi.org/10.5194/acp-13-7183-2013, 2013.

Folberth, G. A., Hauglustaine, D. A., Lathière, J., and Brocheton, F.: Interactive chemistry in the Laboratoire de Météorologie Dynamique general circulation model: model description and impact analysis of biogenic hydrocarbons on tropospheric chemistry, Atmospheric Chemistry and Physics, 6, 2273–2319, https://doi.org/10.5194/acp-6-2273-2006, 2006.

Fouquart, Y. and Bonnel, B.: Computations of solar heating of the earth's atmosphere: A new parameterization, Beitr. Phys. Atmos., 53, 35–62, 1980.

Geels, C., Gloor, M., Ciais, P., Bousquet, P., Peylin, P., Vermeulen, A. T., Dargaville, R., Aalto, T., Brandt, J., Christensen, J. H., Frohn, L. M., Haszpra, L., Karstens, U., Rödenbeck, C., Ramonet, M., Carboni, G., and Santaguida, R.: Comparing atmospheric transport models for future regional inversions over Europe – Part 1: mapping the atmospheric CO2 signals, Atmospheric Chemistry and Physics, 7, 3461–3479, https://doi.org/10.5194/acp-7-3461-2007, 2007.

Giorgetta, M. A., Brokopf, R., Crueger, T., Esch, M., Fiedler, S., Helmert, J., Hohenegger, C., Kornblueh, L., Köhler, M., Manzini, E., Mauritsen, T., Nam, C., Raddatz, T., Rast, S., Reinert, D., Sakradzija, M., Schmidt, H., Schneck, R., Schnur, R., Silvers, L., Wan, H., Zängl, G., and Stevens, B.: ICON-A, the Atmosphere Component of the ICON Earth System Model: I. Model Description, Journal of Advances in Modeling Earth Systems, 10, 1613–1637, https://doi.org/10.1029/2017MS001242, 2018.

Grandpeix, J.-Y., Phillips, V., and Tailleux, R.: Improved mixing representation in Emanuel's convection scheme, Q. J. R. Meteorol. Soc., 130, 3207–3222, https://doi.org/10.1256/qj.03.144, 2004.

Hall, B. D., Crotwell, A. M., Kitzis, D. R., Mefford, T., Miller, B. R., Schibig, M. F., and Tans, P. P.: Revision of the World Meteorological Organization Global Atmosphere Watch (WMO/GAW) CO2 calibration scale, Atmospheric Measurement Techniques, 14, 3015–3032, https://doi.org/10.5194/amt-14-3015-2021, 2021.

Hazan, L., Tarniewicz, J., Ramonet, M., Laurent, O., and Abbaris, A.: Automatic processing of atmospheric CO2 and CH4 mole fractions at the ICOS Atmosphere Thematic Centre, Atmospheric Measurement Techniques, 9, 4719–4736, https://doi.org/10.5194/amt-9-4719-2016, 2016.

Herrington, A. R., Lauritzen, P. H., Lofverstrom, M., Lipscomb, W. H., Gettelman, A., and Taylor, M. A.: Impact of grids and dynamical cores in CESM2.2 on the surface mass balance of the Greenland Ice Sheet, Journal of Advances in Modeling Earth Systems, 14~~n/a~~, e2022MS003192, https://doi.org/10.1029/2022MS003192, 2022~~n.d~~.

Hersbach, H., Bell, B., Berrisford, P., Hirahara, S., Horányi, A., Muñoz-Sabater, J., Nicolas, J., Peubey, C., Radu, R., Schepers, D., Simmons, A., Soci, C., Abdalla, S., Abellan, X., Balsamo, G., Bechtold, P., Biavati, G., Bidlot, J., Bonavita, M., De Chiara, G., Dahlgren, P., Dee, D., Diamantakis, M., Dragani, R., Flemming, J., Forbes, R., Fuentes, M., Geer, A., Haimberger, L., Healy, S., Hogan, R. J., Hólm, E., Janisková, M., Keeley, S., Laloyaux, P., Lopez, P., Lupu, C., Radnoti, G., de Rosnay, P., Rozum, I., Vamborg, F., Villaume, S., and Thépaut, J.-N.: The ERA5 global reanalysis, Quarterly Journal of the Royal Meteorological Society, 146, 1999–2049, https://doi.org/10.1002/qj.3803, 2020.

Hourdin, F., Musat, I., Bony, S., Braconnot, P., Codron, F., Dufresne, J.-L., Fairhead, L., Filiberti, M.-A., Friedlingstein, P., Grandpeix, J.-Y., Krinner, G., LeVan, P., Li, Z.-X., and Lott, F.: The LMDZ4 general circulation model: climate performance and sensitivity to parametrized physics with emphasis on tropical convection, Clim Dyn, 27, 787–813, https://doi.org/10.1007/s00382-006-0158-0, 2006.

34

Hourdin, F., Grandpeix, J.-Y., Rio, C., Bony, S., Jam, A., Cheruy, F., Rochetin, N., Fairhead, L., Idelkadi, A., Musat, I., Dufresne, J.-L., Lahellec, A., Lefebvre, M.-P., and Roehrig, R.: LMDZ5B: the atmospheric component of the IPSL climate model with revisited parameterizations for clouds and convection, Clim Dyn, 40, 2193–2222, https://doi.org/10.1007/s00382-012-1343-y, 2013.

Hourdin, F., Rio, C., Grandpeix, J.-Y., Madeleine, J.-B., Cheruy, F., Rochetin, N., Jam, A., Musat, I., Idelkadi, A., Fairhead, L., Foujols, M.-A., Mellul, L., Traore, A.-K., Dufresne, J.-L., Boucher, O., Lefebvre, M.-P., Millour, E., Vignon, E., Jouhaud, J., Diallo, F. B., Lott, F., Gastineau, G., Caubel, A., Meurdesoif, Y., and Ghattas, J.: LMDZ6A: The Atmospheric Component of the IPSL Climate Model With Improved and Better Tuned Physics, Journal of Advances in Modeling Earth Systems, 12, e2019MS001892, https://doi.org/10.1029/2019MS001892, 2020.

Houweling, S., Aben, I., Breon, F.-M., Chevallier, F., Deutscher, N., Engelen, R., Gerbig, C., Griffith, D., Hungershoefer, K., Macatangay, R., Marshall, J., Notholt, J., Peters, W., and Serrar, S.: The importance of transport model uncertainties for the estimation of CO2 sources and sinks using satellite measurements, Atmos. Chem. Phys., 10, 9981–9992, https://doi.org/10.5194/acp-10-9981-2010, 2010.

ICOS RI, Bergamaschi, P., Colomb, A., De Mazière, M., Emmenegger, L., Kubistin, D., Lehner, I., Lehtinen, K., Lund Myhre, C., Marek, M., Platt, S.M., Plaß-Dülmer, C., Schmidt, M., Apadula, F., Arnold, S., Blanc, P.-E., Brunner, D., Chen, H., Chmura, L., Conil, S., Couret, C., Cristofanelli, P., Delmotte, M., Forster, G., Frumau, A., Gheusi, F., Hammer, S., Haszpra, L., Heliasz, M., Henne, S., Hoheisel, A., Kneuer, T., Laurila, T., Leskinen, A., Leuenberger, M., Levin, I., Lindauer, M., Lopez, M., Lunder, C., Mammarella, I., Manca, G., Manning, A., Marklund, P., Martin, D., Meinhardt, F., Müller-Williams, J., Necki, J., O'Doherty, S., Ottosson-Löfvenius, M., Philippon, C., Piacentino, S., Pitt, J., Ramonet, M., Rivas-Soriano, P., Scheeren, B., Schumacher, M., Sha, M.K., Spain, G., Steinbacher, M., Sørensen, L.L., Vermeulen, A., Vítková, G., Xueref-Remy, I., di Sarra, A., Conen, F., Kazan, V., Roulet, Y.-A., Biermann, T., Heltai, D., Hensen, A., Hermansen, O., Komínková, K., Laurent, O., Levula, J., Pichon, J.-M., Smith, P., Stanley, K., Trisolino, P., ICOS Carbon Portal, ICOS Atmosphere Thematic Centre, ICOS Flask And Calibration Laboratory, ICOS Central Radiocarbon Laboratory, 2023. European Obspack compilation of atmospheric carbon dioxide data from ICOS and non-ICOS European stations for the period 1972-2023: obspack_co2_466_GLOBALVIEWplus_v8.0_2023-04-26. https://doi.org/10.18160/CEC4-CAGK

Jones, M. W., Andrew, R. M., Peters, G. P., Janssens-Maenhout, G., De-Gol, A. J., Ciais, P., Patra, P. K., Chevallier, F., and Le Quéré, C.: Gridded fossil CO2 emissions and related O2 combustion consistent with national inventories 1959-2018, Scientific Data, 8, https://doi.org/10.1038/s41597-020-00779-6, 2021.

Kenneth N. Schuldt, John Mund, Ingrid T. Luijkx, Tuula Aalto, James B. Abshire, Ken Aikin, Arlyn Andrews, Shuji Aoki, Francesco Apadula, Bianca Baier, Peter Bakwin, Jakub Bartyzel, Gilles Bentz, Peter Bergamaschi, Andreas Beyersdorf, Tobias Biermann, Sebastien C. Biraud, Harald Boenisch, David Bowling, Gordon Brailsford, Willi A. Brand, Huilin Chen, Gao Chen, Lukasz Chmura, Shane Clark, Sites Climadat, Aurelie Colomb, Roisin Commane, Sébastien Conil, Cedric Couret, Adam Cox, Paolo Cristofanelli, Emilio Cuevas, Roger Curcoll, Bruce Daube, Kenneth Davis, Martine De Mazière, Stephan De Wekker, Julian Della Coletta, Marc Delmotte, Joshua P. DiGangi, Ed Dlugokencky, James W. Elkins, Lukas Emmenegger, Shuangxi Fang, Marc L. Fischer, Grant Forster, Arnoud Frumau, Michal Galkowski, Luciana V. Gatti, Torsten Gehrlein, Christoph Gerbig, Francois Gheusi, Emanuel Gloor, Vanessa Gomez-Trueba, Daisuke Goto, Tim Griffis, Samuel Hammer, Chad Hanson, László Haszpra, Juha Hatakka, Martin Heimann, Michal Heliasz, Daniela Heltai, Arjan Hensen, Ove Hermanssen, Eric Hintsa, Antje Hoheisel, Jutta Holst, Viktor Ivakhov, Dan Jaffe, Armin Jordan, Warren Joubert, Anna Karion, Stephan R. Kawa, Victor Kazan, Ralph Keeling, Petri Keronen, Jooil Kim, Tobias Kneuer, Pasi Kolari, Katerina Kominkova, Eric Kort, Elena Kozlova, Paul Krummel, Dagmar Kubistin, Casper Labuschagne, David H. Lam, Xin Lan, Ray Langenfelds, Olivier Laurent, Tuomas Laurila,

Thomas Lauvaux, Jost Lavric, Bev Law, Olivia S. Lee, John Lee, Irene Lehner, Kari Lehtinen, Reimo Leppert, Ari Leskinen, Markus Leuenberger, Ingeborg Levin, Janne Levula, John Lin, Matthias Lindauer, Zoe Loh, Morgan Lopez, Chris R. Lunder, Toshinobu Machida, Ivan Mammarella, Giovanni Manca, Alistair Manning, Andrew Manning, Michal V. Marek, Melissa Y. Martin, Giordane A. Martins, Hidekazu Matsueda, Kathryn McKain, Harro Meijer, Frank Meinhardt, Lynne Merchant, N. Mihalopoulos, Natasha Miles, John B. Miller, Charles E. Miller, Logan Mitchell, Stephen Montzka, Fred Moore, Heiko Moossen, Eric Morgan, Josep-Anton Morgui, Shinji Morimoto, Bill Munger, David Munro, Cathrine L. Myhre, Meelis Mölder, Jennifer Müller-Williams, Jaroslaw Necki, Sally Newman, Sylvia Nichol, Yosuke Niwa, Simon O\'Doherty, Florian Obersteiner, Bill Paplawsky, Jeff Peischl, Olli Peltola, Salvatore Piacentino, Jean M. Pichon, Steve Piper, Joseph Pitt, Christian Plass-Duelmer, Stephen M. Platt, Steve Prinzivalli, Michel Ramonet, Ramon Ramos, Enrique Reyes-Sanchez, Scott Richardson, Haris Riris, Pedro P. Rivas, Michael Rothe, Thomas Ryerson, Kazuyuki Saito, Maryann Sargent, Motoki Sasakawa, Bert Scheeren, Martina Schmidt, Tanja Schuck, Marcus Schumacher, Thomas Seifert, Mahesh K. Sha, Paul Shepson, Michael Shook, Christopher D. Sloop, Paul Smith, Martin Steinbacher, Britton Stephens, Colm Sweeney, Lise L. Sørensen, Pieter Tans, Kirk Thoning, Helder Timas, Margaret Torn, Pamela Trisolino, Jocelyn Turnbull, Kjetil Tørseth, Alex Vermeulen, Brian Viner, Gabriela Vitkova, Stephen Walker, Andrew Watson, Ray Weiss, Steve Wofsy, Justin Worsey, Doug Worthy, Dickon Young, Sönke Zaehle, Andreas Zahn, Miroslaw Zimnoch, Rodrigo A. de Souza, Alcide G. di Sarra, Danielle van Dinther, Pim van den Bulk; Multi-laboratory compilation of atmospheric carbon dioxide data for the period 1957-2021; obspack_co2_1_GLOBALVIEWplus_v8.0_2022-08-27; NOAA Earth System Research Laboratory, Global Monitoring Laboratory. ~~http://doi.org/10.25925/20220808~~http://doi.org/10.25925/20220808, 2022~~.~~

Krinner, G., Viovy, N., de Noblet-Ducoudré, N., Ogée, J., Polcher, J., Friedlingstein, P., Ciais, P., Sitch, S., and Prentice, I. C.: A dynamic global vegetation model for studies of the coupled atmosphere-biosphere system, Global Biogeochemical Cycles, 19, https://doi.org/10.1029/2003GB002199, 2005.

Lan, X., J.W. Mund, A.M. Crotwell, M.J. Crotwell, E. Moglia, M. Madronich, D. Neff and K.W. Thoning (2023), Atmospheric Carbon Dioxide Dry Air Mole Fractions from the NOAA GML Carbon Cycle Cooperative Global Air Sampling Network, 1968-2022, Version: 2023-08-28, https://doi.org/10.15138/wkgj-f215

Lauvaux, T., Pannekoucke, O., Sarrat, C., Chevallier, F., Ciais, P., Noilhan, J., and Rayner, P. J.: Structure of the transport uncertainty in mesoscale inversions of CO_2 sources and sinks using ensemble model simulations, Biogeosciences, 6, 1089–1102, https://doi.org/10.5194/bg-6-1089-2009, 2009.

Lin, X., Ciais, P., Bousquet, P., Ramonet, M., Yin, Y., Balkanski, Y., Cozic, A., Delmotte, M., Evangeliou, N., Indira, N. K., Locatelli, R., Peng, S., Piao, S., Saunois, M., Swathi, P. S., Wang, R., Yver-Kwok, C., Tiwari, Y. K., and Zhou, L.: Simulating CH_4 and CO_2 over South and East Asia using the zoomed chemistry transport model LMDz-INCA, Atmospheric Chemistry and Physics, 18, 9475–9497, https://doi.org/10.5194/acp-18-9475-2018, 2018.

Lloret, Z., Cozic, A., Chevallier, F., Remaud, M., & Meurdesoif, Y.: ICOLMDZORINCA CO2 Transport GMD 2023. Zenodo. https://doi.org/10.5281/zenodo.10019679, 2023.

Lott, F., Fairhead, L., Hourdin, F., and Levan, P.: The stratospheric version of LMDz: dynamical climatologies, arctic oscillation, and impact on the surface climate, Clim Dyn, 25, 851–868, https://doi.org/10.1007/s00382-005-0064-x, 2005.

Mellor, G. L. and Yamada, T.: A Hierarchy of Turbulence Closure Models for Planetary Boundary Layers, Journal of the Atmospheric Sciences, 31, 1791–1806, https://doi.org/10.1175/1520-0469(1974)031<1791:AHOTCM>2.0.CO;2, 1974.

Miles, N.L., S.J. Richardson, K.J. Davis, and B.J. Haupt, 2017. In-situ tower atmospheric measurements of carbon dioxide, methane and carbon monoxide mole fraction for the Indianapolis Flux (INFLUX) project, Indianapolis, IN, USA. Data set. Available on-line http://datacommons.psu.edu from The Pennsylvania State University Data Commons, University Park,

765 Pennsylvania, USA. http://dx.doi.org/10.18113/D37G6P
766 Miles, N.L., S.J. Richardson, D.K. Martins, K.J. Davis, T. Lauvaux, B.J. Haupt, and S.K. Miller. 2018. ACT-America: L2 In Situ
767 CO2, CO, and CH4 Concentrations from Towers, Eastern USA. ORNL DAAC, Oak Ridge, Tennessee, USA.
768 https://doi.org/10.3334/ORNLDAAC/1568
769 Mlawer, E. J., Taubman, S. J., Brown, P. D., Iacono, M. J., and Clough, S. A.: Radiative transfer for inhomogeneous
770 atmospheres: RRTM, a validated correlated-k model for the longwave, Journal of Geophysical Research: Atmospheres, 102,
771 16663–16682, https://doi.org/10.1029/97JD00237, 1997.
772 Niwa, Y., Tomita, H., Satoh, M., Imasu, R., Sawa, Y., Tsuboi, K., Matsueda, H., Machida, T., Sasakawa, M., Belan, B., and
773 Saigusa, N.: A 4D-Var inversion system based on the icosahedral grid model (NICAM-TM 4D-Var v1.0) – Part 1: Offline
774 forward and adjoint transport models, Geosci. Model Dev., 10, 1157–1174, https://doi.org/10.5194/gmd-10-1157-2017, 2017.
775 Remaud, M., Chevallier, F., Cozic, A., Lin, X., and Bousquet, P.: On the impact of recent developments of the LMDz
776 atmospheric general circulation model on the simulation of CO2 transport, Geosci. Model Dev., 25, 2018.
777 Rio, C., Hourdin, F., Grandpeix, J.-Y., and Lafore, J.-P.: Shifting the diurnal cycle of parameterized deep convection over land,
778 Geophysical Research Letters, 36, https://doi.org/10.1029/2008GL036779, 2009.
779 Rochetin, N., Grandpeix, J.-Y., Rio, C., and Couvreux, F.: Deep Convection Triggering by Boundary Layer Thermals. Part II:
780 Stochastic Triggering Parameterization for the LMDZ GCM, Journal of the Atmospheric Sciences, 71, 515–538,
781 https://doi.org/10.1175/JAS-D-12-0337.1, 2014.
782 Sakaguchi, K., Harrop, B. E., Leung, L. R., Jang, J., Gettelman, A., Zarzycki, C. M., Lin, G., Zhang, K., and Skamarock, W. C.:
783 The CAM-MPAS model simulations for the HighResMIP experiments, 2020, A090-0014, 2020.
784 Sepulchre, P., Caubel, A., Ladant, J.-B., Bopp, L., Boucher, O., Braconnot, P., Brockmann, P., Cozic, A., Donnadieu, Y.,
785 Dufresne, J.-L., Estella-Perez, V., Ethé, C., Fluteau, F., Foujols, M.-A., Gastineau, G., Ghattas, J., Hauglustaine, D., Hourdin, F.,
786 Kageyama, M., Khodri, M., Marti, O., Meurdesoif, Y., Mignot, J., Sarr, A.-C., Servonnat, J., Swingedouw, D., Szopa, S., and
787 Tardif, D.: IPSL-CM5A2 – an Earth system model designed for multi-millennial climate simulations, Geoscientific Model
788 Development, 13, 3011–3053, https://doi.org/10.5194/gmd-13-3011-2020, 2020.
789 Shepherd, T. G., Semeniuk, K., and Koshyk, J. N.: Sponge layer feedbacks in middle-atmosphere models, Journal of
790 Geophysical Research: Atmospheres, 101, 23447–23464, https://doi.org/10.1029/96JD01994, 1996.
791 Staniforth, A. and Thuburn, J.: Horizontal grids for global weather and climate prediction models: a review, Quarterly Journal of
792 the Royal Meteorological Society, 138, 1–26, https://doi.org/10.1002/qj.958, 2012.
793 Tort, M., Dubos, T., Bouchut, F., and Zeitlin, V.: Consistent shallow-water equations on the rotating sphere with complete
794 Coriolis force and topography, Journal of Fluid Mechanics, 748, 789–821, https://doi.org/10.1017/jfm.2014.172, 2014.
795 Ullrich, P. A., Jablonowski, C., Kent, J., Lauritzen, P. H., Nair, R., Reed, K. A., Zarzycki, C. M., Hall, D. M., Dazlich, D.,
796 Heikes, R., Konor, C., Randall, D., Dubos, T., Meurdesoif, Y., Chen, X., Harris, L., Kühnlein, C., Lee, V., Qaddouri, A., Girard,
797 C., Giorgetta, M., Reinert, D., Klemp, J., Park, S.-H., Skamarock, W., Miura, H., Ohno, T., Yoshida, R., Walko, R., Reinecke,
798 A., and Viner, K.: DCMIP2016: a review of non-hydrostatic dynamical core design and intercomparison of participating models,
799 Geoscientific Model Development, 10, 4477–4509, https://doi.org/10.5194/gmd-10-4477-2017, 2017.
800 Van Leer, B.: Towards the ultimate conservative difference scheme. IV. A new approach to numerical convection, Journal of
801 Computational Physics, 23, 276–299, https://doi.org/10.1016/0021-9991(77)90095-X, 1977.
802 Wagenhäuser, T., Engel, A., and Sitals, R.: Testing the altitude attribution and vertical resolution of AirCore measurements with
803 a new spiking method, Atmospheric Measurement Techniques, 14, 3923–3934, https://doi.org/10.5194/amt-14-3923-2021, 2021.
804 Zheng, T., Feng, S., Davis, K. J., Pal, S., and Morguí, J.-A.: Development and evaluation of CO2 transport in MPAS-A v6.3,
805 Geoscientific Model Development, 14, 3037–3066, https://doi.org/10.5194/gmd-14-3037-2021, 2021.